



Chinese Pharmaceutical Association
Institute of Materia Medica, Chinese Academy of Medical Sciences

Acta Pharmaceutica Sinica B

www.elsevier.com/locate/apsb
www.sciencedirect.com



ORIGINAL ARTICLE

Discovery of novel covalent selective estrogen receptor degraders against endocrine-resistant breast cancer



Yubo Wang^{a,†}, Jian Min^{b,†}, Xiangping Deng^{a,†}, Tian Feng^{a,†},
Hebing Hu^b, Xinyi Guo^a, Yan Cheng^a, Baohua Xie^a, Yu Yang^b,
Chun-Chi Chen^b, Rey-Ting Guo^{b,*}, Chune Dong^{a,c,*},
Hai-Bing Zhou^{a,c,d,*}

^aDepartment of Gynecological Oncology, Zhongnan Hospital of Wuhan University, School of Pharmaceutical Sciences, Wuhan University, Wuhan 430071, China

^bState Key Laboratory of Biocatalysis and Enzyme Engineering, National & Local Joint Engineering Research Center of High-throughput Drug Screening Technology, Hubei Key Laboratory of Industrial Biotechnology, School of Life Sciences, Hubei University, Wuhan 430062, China

^cFrontier Science Center for Immunology and Metabolism, State Key Laboratory of Virology, Provincial Key Laboratory of Developmentally Originated Disease, Key Laboratory of Combinatorial Biosynthesis and Drug Discovery (MOE) and Hubei Province Engineering and Technology Research Center for Fluorinated Pharmaceuticals, Wuhan University, Wuhan 430071, China

^dWuhan Research Center for Infectious Diseases and Cancer, Chinese Academy of Medical Sciences, Zhongnan Hospital of Wuhan University, Wuhan 430071, China

Received 29 March 2023; received in revised form 3 May 2023; accepted 6 May 2023

KEY WORDS

Covalent strategy;
Estrogen receptor
degraders;
Endocrine-resistant breast
cancer;
X-ray crystallography

Abstract Endocrine-resistance remains a major challenge in estrogen receptor α positive (ER α^+) breast cancer (BC) treatment and constitutively active somatic mutations in ER α are a common mechanism. There is an urgent need to develop novel drugs with new mode of mechanism to fight endocrine-resistance. Given aberrant ER α activity, we herein report the identification of novel covalent selective estrogen receptor degraders (cSERDs) possessing the advantages of both covalent and degradation strategies. A highly potent cSERD **29c** was identified with superior anti-proliferative activity than fulvestrant against a panel of ER α^+ breast cancer cell lines including mutant ER α . Crystal structure of ER α -**29c**

*Corresponding authors.

E-mail addresses: guoreyting@hubu.edu.cn (Rey-Ting Guo), cdong@whu.edu.cn (Chune Dong), zhouhb@whu.edu.cn (Hai-Bing Zhou).

[†]These authors made equal contributions to this work.

Peer review under responsibility of Chinese Pharmaceutical Association and Institute of Materia Medica, Chinese Academy of Medical Sciences.

<https://doi.org/10.1016/j.apsb.2023.05.005>

2211-3835 © 2023 Chinese Pharmaceutical Association and Institute of Materia Medica, Chinese Academy of Medical Sciences. Production and hosting by Elsevier B.V. This is an open access article under the CC BY-NC-ND license (<http://creativecommons.org/licenses/by-nc-nd/4.0/>).

complex alongside intact mass spectrometry revealed that **29c** disrupted ER α protein homeostasis through covalent targeting C530 and strong hydrophobic interaction collided on H11, thus enforcing a unique antagonist conformation and driving the ER α degradation. These significant effects of the cSERD on ER α homeostasis, unlike typical ER α degraders that occur directly *via* long side chains perturbing the morphology of H12, demonstrating a distinct mechanism of action (MoA). *In vivo*, **29c** showed potent antitumor activity in MCF-7 tumor xenograft models and low toxicity. This proof-of-principle study verifies that novel cSERDs offering new opportunities for the development of innovative therapies for endocrine-resistant BC.

© 2023 Chinese Pharmaceutical Association and Institute of Materia Medica, Chinese Academy of Medical Sciences. Production and hosting by Elsevier B.V. This is an open access article under the CC BY-NC-ND license (<http://creativecommons.org/licenses/by-nc-nd/4.0/>).

1. Introduction

Breast cancer (BC) is one of the most prevalent malignancies in women globally, with approximately 70% of patients diagnosed as ER α positive (ER α^+)^{1,2}. The generally recognized therapeutic strategy is to block ER α signaling for ER α^+ BC^{3,4}. Over the past decades, standard-of-care (SOC) endocrine therapies have been developed to antagonize oncogenic ER α function in the clinic⁵. SOC for BC includes aromatase inhibitors (AIs, *e.g.*, **1a** letrozole, **1b** exemestane) that block estrogen hormone synthesis and selective estrogen receptor modulators (SERMs, *e.g.*, **2a** tamoxifen, **2c** raloxifene, **2d** lasofoxifene) (Fig. 1A and B) that antagonize ER α signaling pathway⁶. Although current therapies have shown considerable clinical benefit in the treatment of ER α^+ BC, the increased intrinsic and acquired resistance became a major problem⁷. Statistically, about 25% of patients develop resistance under the pressure of endocrine therapy. In endocrine-resistant settings, up to 90% of breast tumor progression rely on ligand-independent activation of transcription by ER α mutations⁸. Thus, targeted protein degradation (TPD) therapies capable of removing the proteins, such as selective estrogen receptor degraders (SERDs) or proteolysis targeting chimeras (PROTACs) would be an ideal strategy against the endocrine-resistant BC^{9–12}. Different from the catalytic mechanism of PROTACs, SERDs achieve antagonism by interfering ER α homeostasis and enforcing programmed degradation¹³. Fulvestrant (Ful, **3a**), the only FDA-approved SERD, presents limited applications due to poor pharmacokinetic (PK) properties¹⁴.

Second-generation SERDs have been developed to overcome drug resistance with improved pharmacokinetic profiles than Ful (Fig. 1C)^{15,16}. The investigation of GDC0810 (**3b**) was terminated in a phase II due to insufficient clinical benefits. AZD9496 (**3c**) and LSZ102 (**3d**) entered phase I clinical trials and was halted due to intolerable side effects or unsatisfying objective response rate (ORR)⁹. Four oral SERDs: AZD9833 (**3f**), GDC9545 (**3g**), SAR439859 (**3h**) and RAD1901 (**3e**) are currently under evaluation in phase III clinical trials for advanced BC¹⁷. Characteristically, the second-generation SERDs relied on a single mechanism for their drug design strategy, with extended bulky side chains completely displace helix 12 (H12), leading to exposure of the hydrophobic surface, misfolding of ER α proteins, and subsequent proteasomal degradation⁸. Mutations in the ER gene (*ESR1*) tend to occur in hot spots that encode amino acids 536, 537 or 538 of ligand-binding domain (LBD), and the most frequent ESR1 mutations are Y537S and D538G¹⁸. Therefore, there is a challenge for SERDs design to balance H12 displacement-driven

degradation with stabilizing effects of the H12 mutation derived ligand-independent activation¹⁹.

Comprehensive structural-biochemical investigations demonstrated that both mutations of ER α ligand binding pocket (LBP) had significantly reduced affinities of ligands and led to incomplete inhibition of target protein cascade with its downstream signaling²⁰. Recent studies have demonstrated the success of covalent inhibitors to block and evade mutational events and maintain potency against mutation targets²¹. By covalent targeting, high binding affinity and selectivity were obtained^{22–24}. Based on the process and underlying mechanisms of the ESR1 mutations, mutation-induced conformational change is thought to reduce ligand affinity for ER α ²⁵. Compounds H3B-5942 (**4a**) and H3B-6545 (**4b**), are the first-reported selective estrogen receptor covalent antagonists (SERCAs)^{26,27}. H3B-6545 was entered into phase I/II trials (NCT03250676) and the clinical data showed a median response duration of 7.6 months and an objective response rate (ORR) of 17%²⁸. Although **4a–b** showed robust ER α antagonism by covalently targeting cysteine-530 (C530), they were reported no degradation ability to ER α ^{26,27}.

Inspired by the covalent strategy that could irreversibly fix wild-type or mutant ER α in the antagonist state, we aim to identify a novel ER α degradation mode that will resolve the challenges of low binding affinity for mutant ER α and balancing H12 displacement-driven degradation with stabilizing effects of the ligand-independent activation of H12 mutation. Previously, our group has developed a novel 7-oxabicyclo[2.2.1]heptane core skeleton-based compound library. Among them, certain compounds exhibited full antagonism and ER α degradation by reposition of helix 11 (H11) within the ER α ligand-binding pocket (LBP), referred as indirect antagonism^{29–32}. Whereas C530 located at H11 serves as a covalent target of the ER α LBP, we hypothesized that the combination of covalent and degradation strategies can be utilized on the 7-oxabicyclo[2.2.1]heptane core skeleton, thus allowing the covalent warhead to adopt novel degradation associated with noncanonical conformations³³. Moreover, the degradation strategy is to address the compensatory increase in targeting protein expression that leads to incomplete inhibition of targeting protein cascade with its downstream signaling²⁰. By covalently enhancing the destabilizing potency of the antagonist against the receptor, it enables the ER α to shift the equilibrium toward an unstable antagonistic conformation in the mutational setting. Additionally, the utilization of covalent strategy can improve the ER α ligand efficiency, thus reducing idiosyncrasy toxicity (IDT) through smaller and less frequent dosing regimens²¹.

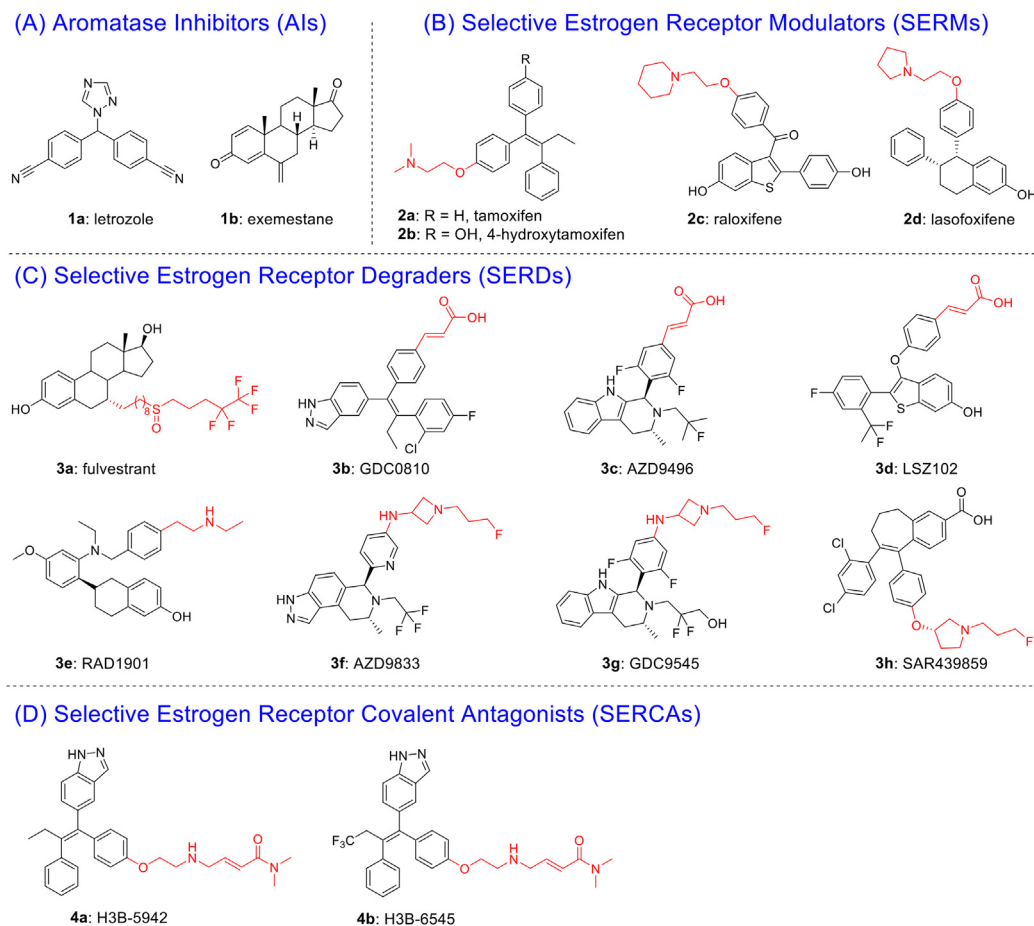


Figure 1 (A, B) Representative AIs and SERMs. (C) Representative SERDs with acidic or basic side chains and (D) SERCAs with electrophilic warheads interaction with C530.

Given that the ER-LBD is plasticity³⁴ and cysteine reactivity varies among different proteins^{35,36}, the crystal structures of *exo*-5,6-bis(4-hydroxyphenyl)-7-oxabicyclo[2.2.1]hept-5-ene-2-sulfonic acid phenyl ester (OBHS) or OBH-sulfonamide (OBHSA) complexed with ER α suggested the accessibility to introduce a covalent warhead targeting C530 of H11 (Figs. 2 and 3). Six most reported cysteine targeting covalent fragments were selected representing Michael-type nucleophilic and substitution nucleophilic warheads²¹, which allowed to build a focused compounds library with a diverse set of covalent fragments (Fig. 2). Systematic structure–activity relationship (SAR) studies indicated that compound **29c** with an OBHSA scaffold had excellent full antagonistic activity and degradability of ER α in Tam-resistant or mutant BC cell lines, as well as potent tumor inhibition in MCF-7 BC xenograft models *in vivo*. Analysis of the crystal structure of ER α –**29c** complex and intact mass spectrometry revealed that **29c** disrupted ER α protein homeostasis through covalent targeting C530 and strong hydrophobic interaction clashed on H11, thus enforcing a unique antagonist conformation and driving the ER α degradation. Herein, we report the discovery of novel covalent selective estrogen receptor degraders (cSERDs) for the treatment of ER α ⁺ BC. This study suggests that cSERDs may represent a new option for overcoming clinical endocrine resistance against ER α ⁺ BC.

2. Results and discussion

2.1. Chemistry

Firstly, we developed a diversity-oriented and functionally synthesis pathway utilizing Diels–Alder reaction to generate a focused set of covalent compounds with the incorporation of distinct structure and chemotype warheads (Schemes 1–3). Next, covalent derivatives based on the OBHS or OBHSA scaffold were obtained through Diels–Alder reaction by a variety of furan derivatives reacted with different warheads (**24a–f**) and various sulfonamide dienophiles (**27a–b**, **17a–j**), or 3,4-bis(4-hydroxyphenyl) furan (**25**) and dienophiles with different warheads (**13a–f**, **17k**) (Scheme 3). Synthesis of key intermediates **11**, **23**, **25** and **27** have been reported in our previous work^{30,31,37}. For details, the synthesis of various vinyl sulfonates **13a–f** were prepared by the reaction of corresponding acyl chloride with compound **11** under basic reaction conditions (Scheme 1A). Relevant systematic works indicated that the sulfonamide motif and *para* substitution of the benzenesulfonic group played significant roles in the ER α binding affinities and degradation activity of the OBHSA derivatives³⁸. Thus, the synthesis of Series III mainly focused on further SAR *via* the N-substitution and phenyl-substitution of dienophiles. The intermediates of sulfonamide

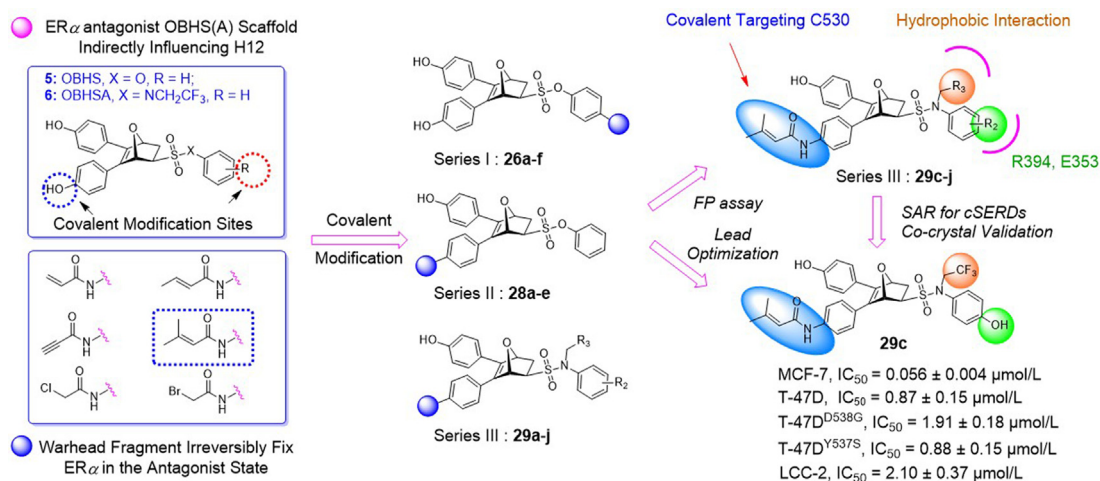


Figure 2 Design strategy of novel covalent SERDs.

dienophiles **17a–j** were prepared according to previous work (Scheme 1B)³⁷. Notably, *ortho*-substituted phenyl of sulfonamide derivatives could not be accessible using this route, possibly due to the large steric hindrance of methoxy group. Compound **17k** was obtained by the reaction of 3,3-dimethylacryloyl chloride under basic conditions.

The general synthetic route of compound **23** was described in Scheme 2. The furan derivatives **24a–f** containing the covalent warheads were carefully prepared by the reaction of corresponding acyl chloride under basic reaction conditions at 0 °C.

The target products were obtained *via* Diels–Alder reaction as shown in Scheme 3. Generally, the final compounds were formed as racemates in thermodynamically favored *exo* configuration²⁹. In addition, compounds **26a–f** of Series I had no regioisomers due to the symmetrical structure of the furan derivative **25**, while compounds **28a–f** of Series II were considered a mixture of regional isomers and, despite our best efforts, they were inseparable. For compounds **29a–m** of Series III, most compounds showed high stereoselectivity in the cyclic addition reaction and trace amounts of regioisomers could be detected by TLC. To investigate the effect of regioisomers on the biological activities, we also isolated the regioisomers **29c'** of the candidate compound **29c** by scaling up the reaction to the grams and performed biological evaluation separately. The characterization of the regioisomers **29c** and **29c'** was provided in Supporting Information (Supporting Information Fig. S1). In addition, the saturated

analog **29k** and the unmodified **29l** were used as negative controls to verify the effect of pharmacophore group of the “Michael receptor”.

2.2. Evaluation the optimal covalent binding mode and the selectivity of ER isoforms

To initiate structure-based drug design, crystal structure of OBHS (PDB: 4ZN9, yellow) and OBHSA (PDB: 5KCW, pink) in complexed with ER α LBD were superimposed (Fig. 3)^{39,40}. The A-ring phenol groups were highly overlaid and pivotal H-bond interactions with two key residues (E353, R394) were observed. The F ring clashed with His524 in the H11 main chain, indirectly changing the stability of H12 in the agonist conformation. Besides, the tight hydrogen-bonding between S537 in the Y537S mutant and D351 on Helix 3 (H3) was also observed⁴¹. The binding modes of OBHS and OBHSA with ER α provides two rational covalent modification sites (Fig. 3). We hoped to launch a set of covalent warheads to these two sites for enhanced covalent degradation. Since cysteine reactivity varies among different proteins, we used a competitive FP assay to quickly screen a diverse set of covalent fragments⁴². The relative binding affinities (RBA) of all compounds were determined and reported in Table 1. These affinities are discussed as RBA values, where estradiol has an affinity of 100% (K_i values, calculated from RBA values, are also given in Table 1). Different from previous studies, our work

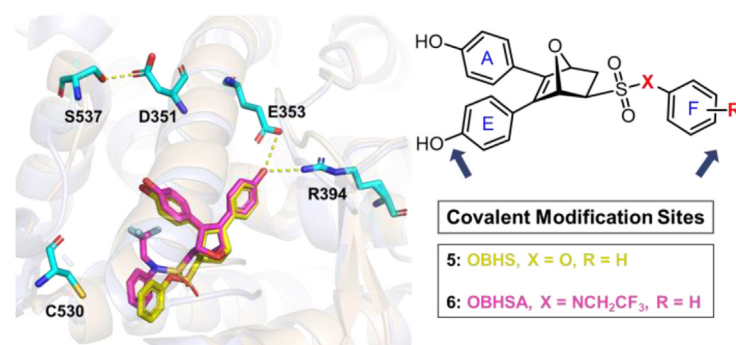
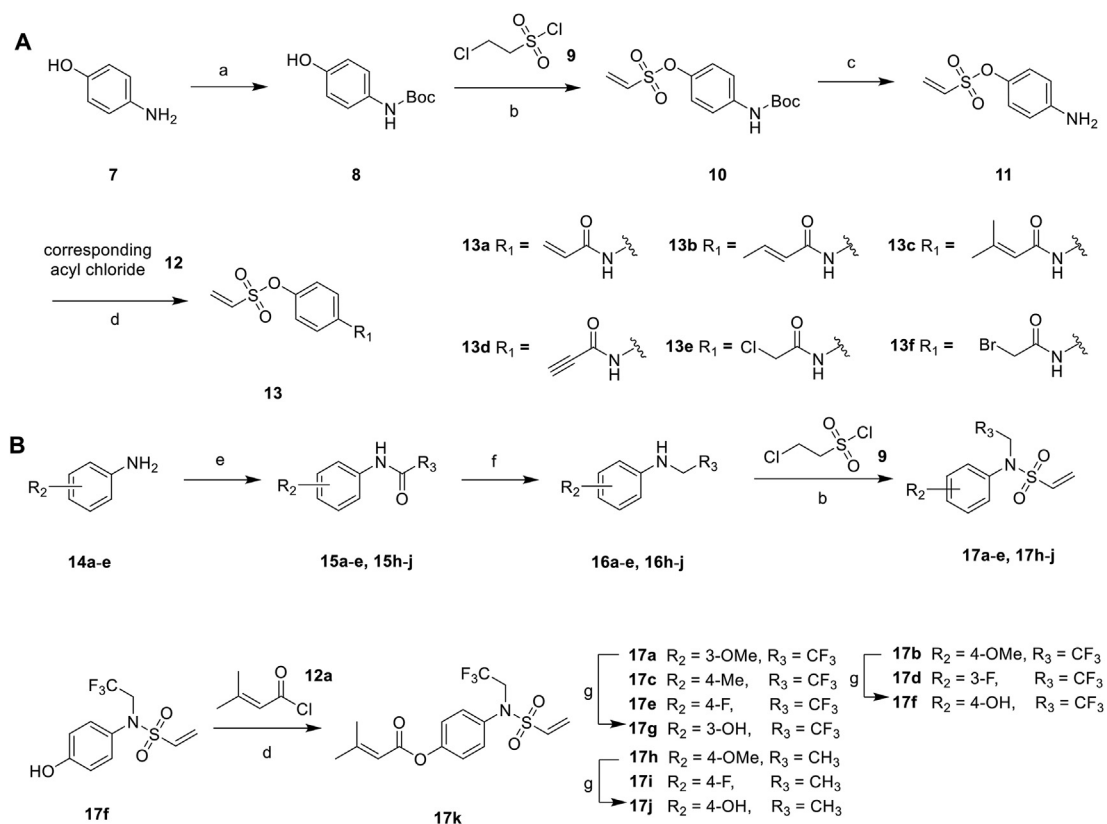


Figure 3 Superimposition of crystal structure of OBHS (PDB: 4ZN9, yellow) and OBHSA (PDB: 5KCW, pink) ER α in complexed with ER α LBD. Key residues were shown as sticks (cyan). H-bonds were represented by dotted yellow lines.

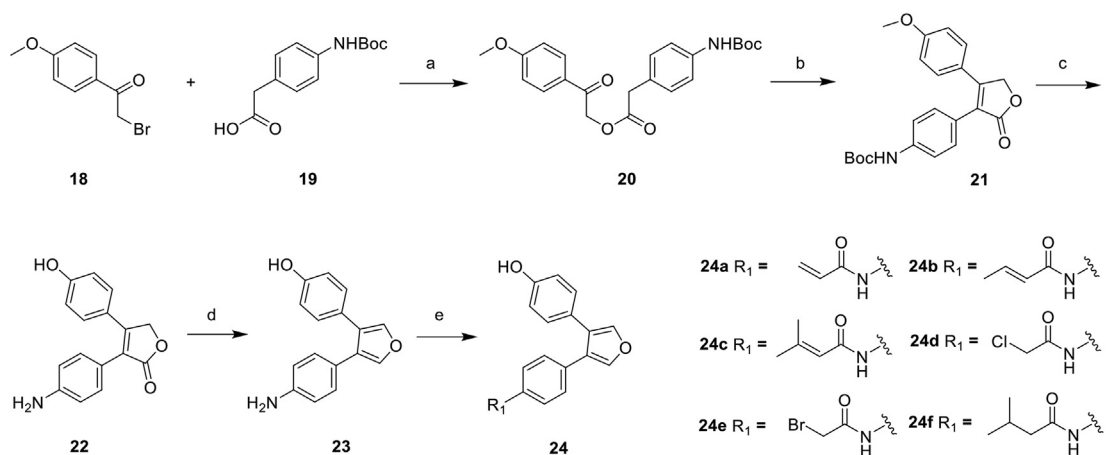


Scheme 1 Synthesis of dienophiles **13a–f** and **17a–k**. Reagents and conditions: (a) Boc_2O , TEA, DCM, 25 °C, 12 h; (b) TEA, DCM, 25 °C, 2 h; (c) TFA, DCM, 25 °C, 2 h; (d) TEA, THF, 0 °C, 2 h; (e) **15a–e**: Trifluoroacetic anhydride, DCM, 25 °C, 3 h; **15h–j**: Acetic anhydride, DCM, 25 °C, 3 h; (f) $(\text{CH}_3)_2\text{S}\cdot\text{BH}_3$, THF, –78 °C, 12 h. (g) BBr_3 , DCM, –78 °C, 12 h.

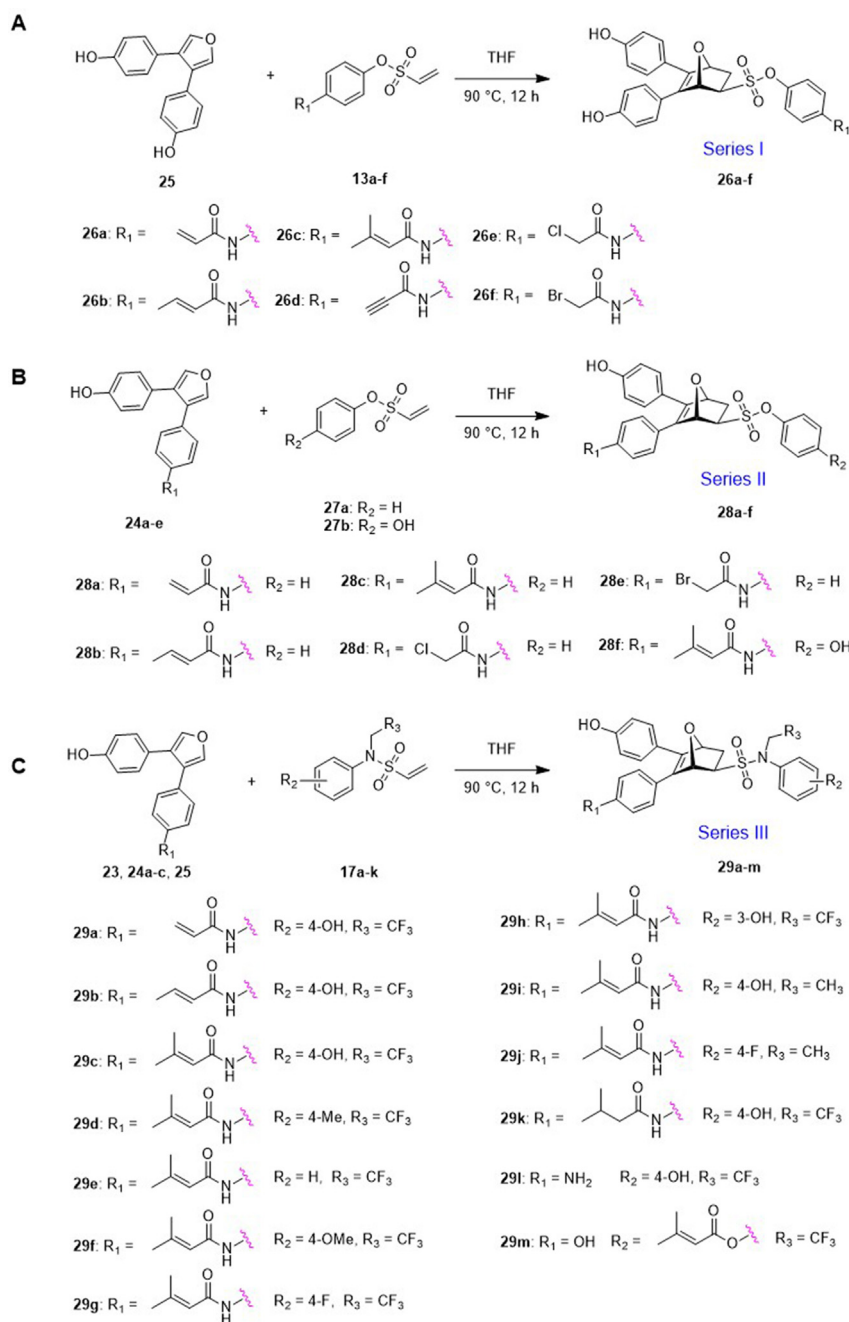
was not only to compare the reactivity of warheads, but also to investigate the accessibility of a covalent set of targeted cysteines of $\text{ER}\alpha$. Thus, RBA values could indicate the preliminary information about covalent binding capacity and efficiency of the target compounds to $\text{ER}\alpha$.

Although RBA values of compounds **26a–f** with covalent warhead on the sulfonate benzene ring of the OBHS skeleton were lower than that of lead compound OBHS (Table 1, entries 1–6 vs

27), compounds **26a–c** ($\text{RBA}^{\text{ER}\alpha} = 3.28\%–8.04\%$) showed potential tolerance and accessibility to covalent binding pocket of $\text{ER}\alpha$. Series II was to explore the effects on binding affinity by changing the covalent modification site. The binding affinities of compounds **28a–c** had a sharp improvement compared with Series I (Table 1, entries 7–9 vs 1–3). In addition, binding affinities of compounds **29a–c** were also significantly improved compared with **28a–c** when changing OBHS to OBHSA scaffold. Among



Scheme 2 Synthesis of furan derivatives **24a–f**. Reagents and conditions: (a) TEA, CH_3CN , 25 °C, 12 h; (b) NaH, DMSO, 25 °C, 2 h; (c) BBr_3 , DCM, –20 °C, 12 h; (d) DIBAL-H, THF, –78 °C, 12 h; (e) TEA, THF, 0 °C, 2 h.

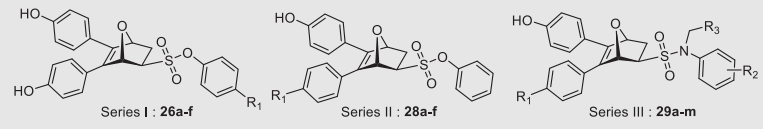


Scheme 3 Synthesis of target compounds **26a–f**, **28a–f** and **29a–m**.

them, compound **29c** with a warhead of 3,3-dimethylacrylamido possessed the highest ER α binding affinity as 30.44%, while the RBA value of the corresponding regioisomer **29c'** was only 15.12% (Table 1, entries 15 vs 16). To conduct further SAR studies, compounds **29d–m** were obtained by the above synthetic route (Scheme 3B) and RBA values were summarized in Table 1 (entries 17–26). Compounds **29d–h** exhibited significantly decreased RBA values to ER α when the *para*-hydroxyl group was replaced. Notably, no-covalent compounds **29k** and **29l** showed significantly decreased the binding affinity of ER α (Table 1, entries 24 and 25 vs 15 and 16).

2.3. Potent antiproliferative activity in ER α^{WT} and ER α^{MUT} breast cancer cell lines

To further investigate reactivity and selectivity of warhead, we evaluated the effects of all target compounds on cell viability of MCF-7 cells. Results expressed as IC₅₀ were summarized in Table 2, and both compounds **5** (OBHS) and **6a** (a derivative of OBHSA, X = NCH₂CF₃, R = 4-OH) were used as the control. In details, compounds **26a–e** of Series I (Table 2, entries 1–5) obtained by introducing a covalent warhead into the sulfonate benzene ring of the OBHS backbone had weak inhibitory activities against

Table 1 Relative binding affinity (RBA) and K_i of all compounds to ER α and ER β ^a.


Entry	Compd.	R ₁	R ₂	R ₃	K_i (nmol/L)		RBA (%)		α/β ratio
					ER α	ER β	ER α	ER β	
1	26a		/	/	0.34	1.73	8.04 ± 0.87	3.86 ± 0.34	2.08
2	26b		/	/	0.58	16.68	4.77 ± 0.16	0.40 ± 0.05	11.93
3	26c		/	/	0.84	5.09	3.28 ± 0.17	1.31 ± 0.66	2.50
4	26d		/	/	3.25	13.61	0.85 ± 0.08	0.49 ± 0.04	1.73
5	26e		/	/	2.71	12.13	1.02 ± 0.13	0.55 ± 0.02	1.85
6	26f		/	/	0.34	1.73	8.04 ± 0.37	3.86 ± 0.34	2.08
7 ^b	28a		/	/	0.15	5.61	18.55 ± 0.34	1.19 ± 0.27	15.59
8 ^b	28b		/	/	0.2	0.64	14.08 ± 0.25	10.40 ± 0.23	1.35
9 ^b	28c		/	/	0.12	7.41	22.13 ± 0.92	0.90 ± 0.25	24.59
10 ^b	28d		/	/	0.8	7.25	3.46 ± 0.02	0.92 ± 0.17	3.76
11 ^b	28e		/	/	0.29	18.53	9.44 ± 0.40	0.36 ± 0.03	26.22
12 ^b	28f		4-OH	/	0.35	2.03	7.93 ± 0.34	3.29 ± 0.25	2.41
13	29a		4-OH	CF ₃	0.14	0.99	20.03 ± 0.25	6.74 ± 0.21	2.97
14	29b		4-OH	CF ₃	0.14	10.59	19.82 ± 0.19	0.63 ± 0.14	31.46
15	29c		4-OH	CF ₃	0.09	10.93	30.44 ± 1.13	0.61 ± 0.11	49.90
16 ^c	29c'		4-OH	CF ₃	0.18	3.25	15.12 ± 0.31	2.05 ± 0.45	7.37
17	29d		4-Me	CF ₃	0.43	4.87	6.49 ± 0.21	1.37 ± 0.11	4.74
18	29e		H	CF ₃	0.29	23.82	9.50 ± 0.09	0.28 ± 0.05	33.9
19	29f		4-OMe	CF ₃	0.19	4.07	14.48 ± 0.65	1.64 ± 0.45	8.83
20	29g		4-F	CF ₃	0.37	6.54	7.52 ± 0.29	1.02 ± 0.13	7.37
21	29h		3-OH	CF ₃	0.35	15.16	7.89 ± 0.11	0.44 ± 0.02	17.93
22	29i		4-OH	CH ₃	0.09	1.3	29.85 ± 1.09	5.12 ± 0.39	5.83
23	29j		4-OMe	CH ₃	0.63	13.08	4.36 ± 0.33	0.51 ± 0.09	8.55
24	29k		4-OH	CF ₃	1.15	4.6	2.41 ± 0.21	1.45 ± 0.12	1.66
25 ^b	29l	NH ₂	4-OH	CF ₃	1.14	2.84	2.43 ± 0.27	2.35 ± 0.33	1.03
26	29m	OH		CF ₃	0.36	8.78	7.77 ± 0.43	0.76 ± 0.15	10.22
27	5				0.33	2.29	8.25 ± 0.67	2.91 ± 0.55	1.41
28 ^d	6a				0.34	1.73	1.05 ± 0.16	0.10 ± 0.02	10.5

^aRelative binding affinity (RBA) values are the mean ± SD of at least three parallel tests. The RBA values: $IC_{50}^{estradiol}/IC_{50}^{compound} \times 100 \pm$ the range (RBA^{estradiol} = 100%). A high RBA means that the compound binds well to the ER and a low RBA means that the compound binds poorly to the ER. $K_i = (100/RBA) \times K_d$. For estradiol, the K_d value was 2.76 and 6.67 nmol/L for ER α and ER β , respectively.

^bSeries II compounds were mixtures of regioisomers.

^cCompound **29c'** was regioisomer of **29c**.

^d**6a** was a derivative of OBHSA, X = NCH₂CF₃, R = 4-OH.

Table 2 The cell viability of the target compounds on MCF-7, T-47D, T-47D^{Y537S} and T-47D^{D538G} cell lines (IC₅₀, μmol/L)^a.

Entry	Compd.	R ₁	R ₂	R ₃	MCF-7 (μmol/L)	T-47D (μmol/L)	T-47D ^{D538G} (μmol/L)	T-47D ^{Y537S} (μmol/L)
1	26a		/	/	7.72 ± 0.64	>31	>31	27.22 ± 0.73
2	26b		/	/	9.18 ± 0.95	19.38 ± 0.54	>31	>31
3	26c		/	/	3.16 ± 0.63	15.84 ± 0.68	8.75 ± 0.25	12.02 ± 0.40
4	26d		/	/	1.79 ± 0.40	6.91 ± 0.29	9.33 ± 0.46	8.93 ± 0.25
5	26e		/	/	3.42 ± 0.32	8.20 ± 0.36	7.86 ± 0.37	8.85 ± 0.61
6	26f		/	/	0.50 ± 0.30	9.11 ± 0.21	>31	>31
7 ^b	28a		/	/	5.07 ± 0.71	>31	>31	>31
8 ^b	28b		/	/	0.44 ± 0.11	25.58 ± 0.98	17.13 ± 0.65	>31
9 ^b	28c		/	/	0.35 ± 0.02	24.92 ± 0.77	17.63 ± 0.89	>31
10 ^b	28d		/	/	0.66 ± 0.12	13.35 ± 0.77	>31	>31
11 ^b	28e		/	/	1.10 ± 0.14	19.72 ± 0.32	>31	>31
12 ^b	28f		4-OH	/	0.93 ± 0.19	8.53 ± 0.12	>31	9.11 ± 0.35
13	29a		4-OH	CF ₃	0.18 ± 0.05	2.85 ± 0.29	5.55 ± 0.24	>31
14	29b		4-OH	CF ₃	0.36 ± 0.04	5.12 ± 0.33	>31	>31
15	29c		4-OH	CF ₃	0.056 ± 0.004	0.87 ± 0.15	1.91 ± 0.18	0.88 ± 0.15
16 ^c	29c'		4-OH	CF ₃	0.95 ± 0.11	5.52 ± 0.27	5.00 ± 0.36	4.05 ± 0.27
17	29d		4-Me	CF ₃	0.75 ± 0.21	8.33 ± 0.22	>31	>31
18	29e		H	CF ₃	0.66 ± 0.12	5.10 ± 0.32	5.18 ± 0.31	1.79 ± 0.17
19	29f		4-OMe	CF ₃	0.094 ± 0.001	8.58 ± 0.36	8.53 ± 0.47	>31
20	29g		4-F	CF ₃	0.64 ± 0.10	5.28 ± 0.23	7.82 ± 0.47	>31
21	29h		3-OH	CF ₃	0.98 ± 0.35	3.92 ± 0.01	2.84 ± 0.14	2.99 ± 0.22
22	29i		4-OH	CH ₃	0.071 ± 0.027	3.49 ± 0.06	4.25 ± 0.19	1.89 ± 0.17
23	29j		4-OMe	CH ₃	0.29 ± 0.03	7.92 ± 0.19	8.25 ± 0.45	12.72 ± 0.53
24	29k		4-OH	CF ₃	1.06 ± 0.19	>31	>31	>31
25	29l		4-OH	CF ₃	3.17 ± 0.33	8.11 ± 0.37	>31	>31
26	29m			CF ₃	0.16 ± 0.04	7.66 ± 0.60	3.68 ± 0.39	3.31 ± 0.34
27 ^d	6a				0.25 ± 0.10	>31	>31	>31
28	4-OHT				0.67 ± 0.08	1.95 ± 0.20	9.13 ± 0.60	8.90 ± 0.28
29	Ful				0.14 ± 0.05	1.76 ± 0.06	3.92 ± 0.22	2.22 ± 0.17

^aValues are the mean ± SD of at least three parallel tests.^bSeries II compounds were mixtures of regioisomers.^cCompound **29c'** was regioisomer of **29c**.^d**6a** was a derivative of OBHSA, X = NCH₂CF₃, R = 4-OH.

MCF-7 cells (IC₅₀ > 0.5 μmol/L). However, in Series II, compounds **28a–d** showed significantly improved inhibitory activity on MCF-7 cells when the warhead was introduced into the phenol ring of the OBHS backbone. Notably, relatively good inhibitory

activity was observed for the compound **28c** with 3,3-dimethylacrylamido as warhead. Combining with the results of the RBA assay, we could reasonably infer the chemotype and loading position of covalent warhead on the carrier of oxygen-

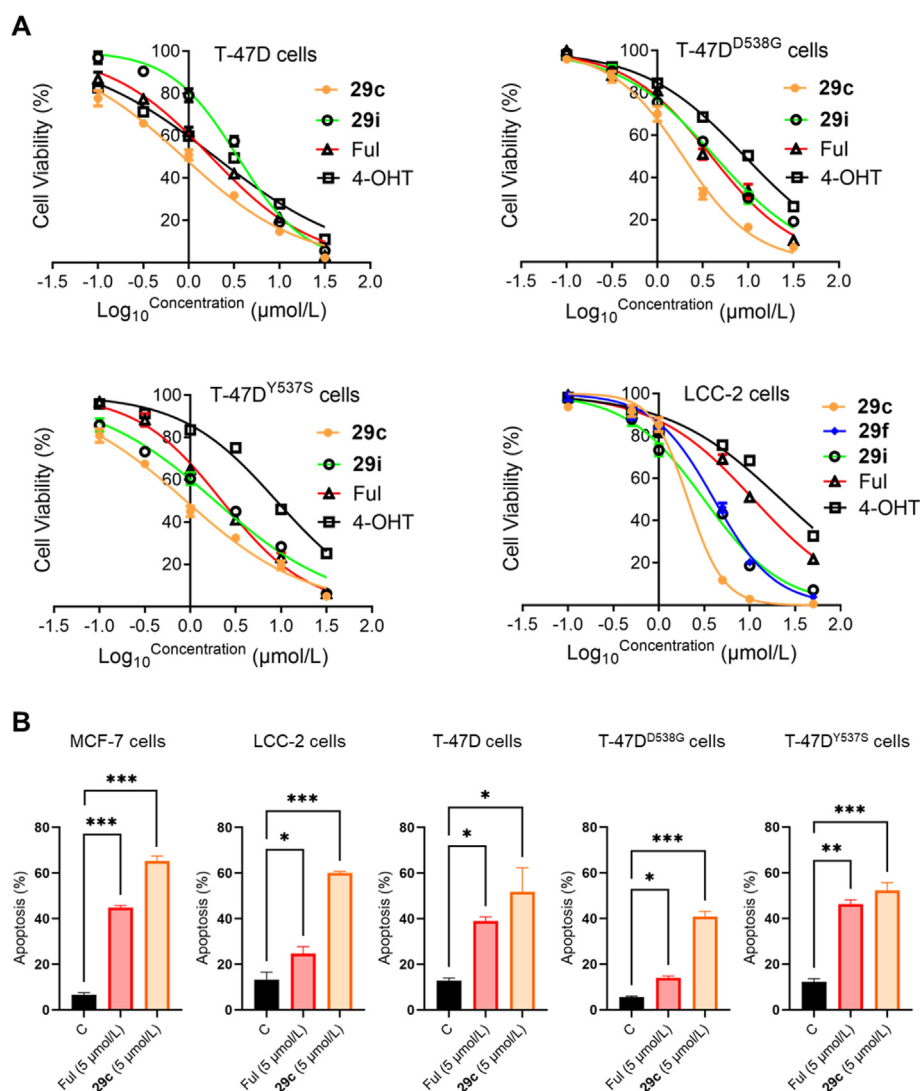
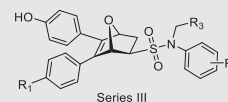


Figure 4 (A) Cell viability assays of key compounds and positive controls in ER α^+ BC cell lines including T-47D cells, T-47D^{D538G} cells, T-47D^{Y537S} cells and LCC-2 cells; (B) Compound **29c** induced MCF-7, LCC-2, T-47D, T-47D^{D538G} and T-47D^{Y537S} cells apoptosis. Cells were exposed to Ful or **29c** for 48 h *** $P < 0.001$, ** $P < 0.01$ and * $P < 0.05$.

bridged bicycloheptene-like structure. Next, the resulting compounds were investigated by shifting optimized covalent warhead to the OBHSA vectors for a series of exemplary compounds **29a–m** (Series III). Among them, compound **29c** ($IC_{50} = 0.056 \mu\text{mol/L}$) displayed the best potency and efficacy against MCF-7 cell line, which was 12- and 2.5-fold higher than positive controls 4-hydroxytamoxifen (4-OHT) and fulvestrant (Ful), respectively (Table 2, entries 15 vs 28 and 29). Compounds **29a–b**, **29k** and **29l** exhibited significantly decreased anti-proliferative potency compared with compound **29c** (Table 2, entries 15 vs 13–14, 24–25), suggesting that the covalent warhead fragment of 3,3-dimethylacrylamido was critical for the inhibitory activity of MCF-7 cells. On the other hand, in comparison with compounds **29c'** and **29k**, we reconfirmed that the 3,3-dimethylacrylamido was the best covalent warhead and its appropriate modification site of OBHSA vectors was also beneficial for good inhibitory activity. Meanwhile, further structure–activity relationship study

Table 3 Cell viability assays on tamoxifen-resistant LCC-2 cell lines (IC_{50} , $\mu\text{mol/L}$)^a.



Entry	Compd.	R ₁	R ₂	R ₃	LCC-2 ($\mu\text{mol/L}$)
1	29c		4-OH	CF ₃	2.10 ± 0.37
2	29f		4-OMe	CF ₃	15.09 ± 1.37
3	29i		4-OH	CH ₃	4.07 ± 0.13
4	4-OHT				22.22 ± 1.93
5	Ful				11.04 ± 0.45

^aValues are the mean ± SD of at least three parallel tests.

Table 4 Transcriptional activity of selected compounds for ER α and ER β ^a.

Entry	Compd.	Agonist mode				Antagonist mode			
		ER α		ER β		ER α		ER β	
		EC ₅₀ (μ mol/L)	Eff (%E ₂)	EC ₅₀ (μ mol/L)	Eff (%E ₂)	IC ₅₀ (μ mol/L)	Eff (%E ₂)	IC ₅₀ (μ mol/L)	Eff (%E ₂)
1	29c	—	5 \pm 1	—	19 \pm 1	0.023	76 \pm 1	—	27 \pm 2
2	29f	4.91	65 \pm 5	—	9 \pm 2	0.21	35 \pm 2	—	13 \pm 1
3	29i	—	15 \pm 2	—	34 \pm 2	0.066	62 \pm 5	1.02	78 \pm 2
4	4-OHT	—	—	—	—	0.039	43 \pm 2	—	11 \pm 3
5	Ful	—	—	—	—	0.013	80 \pm 2	0.22	73 \pm 1
6 ^b	29c	—	2 \pm 1	—	—	0.29	33 \pm 2	—	—
7 ^b	Ful	—	—	—	—	0.027	71 \pm 2	—	—

^aThe luciferase activity are standardized in HEK-293T cells (control as 0% and 10 nmol/L E₂ as 100%). The values are mean \pm SD of at least three independent determinations and the missing parts cannot be accurately determined.

^b**29c** and Ful were evaluated for ER α C530S mutant transcriptional activities in HEK-293T cells.

indicated that substituents R₂ and R₃ were essential for their inhibitory activity against MCF-7 cell lines. For instance, when changing the R₂ group from 4-OH to 3-OH, 4-F or 4-OMe, the anti-proliferative activity of derivatives **29e–h** decreased (Table 2, entries 18–21). For compounds **29i** and **29j**, the replacement of CF₃ with CH₃ group would decrease inhibitory activity on MCF-7 cells (Table 2, entries 15 vs 22 and 19 vs 23).

In addition, the toxicity of these compounds in normal breast cell line MCF-10A was investigated. The IC₅₀ values and therapeutic index (TI) were summarized in Supporting Information Table S1. The results indicated that the focused compounds **29c**, **29f** and **29i** displayed nanomolar activity against MCF-7 with IC₅₀ values in the range of 0.056–0.094 μ mol/L. Although these compounds showed cytotoxic symptoms, the values of TI were 145.1, 54.89 and 122.82, respectively, which were superior to 4-OHT (TI = 32.09) and inferior to Ful (TI > 357.1). Among them, compound **29c** exhibited excellent potency against BC.

Having demonstrated a significant antiproliferative activity of the covalent derivatives in the MCF-7 cell lines, above compounds were also evaluated against another wide-type ER α (ER α ^{WT}) T-47D cell line and mutant ER α (ER α ^{MUT}) containing T-47D^{Y537S} and T-47D^{D538G} cell lines (Table 2). It was found that compounds **29c**, **29h** and **29i** showed better antiproliferation activity than other target compounds. Interestingly, compound **29c** exhibited good activity in T-47D, T-47D^{Y537S} and T-47D^{D538G} cells, 2- to 2.5-fold higher than Ful (Fig. 4A). The decrease in potency of compounds **29e** and **29i** further confirmed that R₂ = 4-OH and R₃ = CF₃ group were vital to improved antiproliferative activity.

Next, **29c** was further characterized in tamoxifen-resistant LCC-2 cells (Table 3). Compound **29c** exhibited better anti-proliferation activity against 4-OHT and Ful. In brief, compound **29c** is a promising covalent SERD against a panel of ER α ⁺ BC cell lines.

Given that **29c** showed good anti-proliferation activity in the above cell lines, we explored the ability of **29c** to induce apoptosis in cell lines by flow cytometry (Supporting Information Fig. S3). Cells were treated with or without 5 μ mol/L **29c** and 5 μ mol/L Ful served as positive control. As shown in Fig. 4B, **29c** significantly induced apoptosis in ER α ^{WT} and ER α ^{MUT} BC cell lines.

2.4. ER transcription activation assays

Compounds **29c**, **29i** and **29f** were evaluated for ER transcriptional activities in HEK-293T cells. The results are summarized

in Table 4, and dose–response curves of representative ligands were shown in Supporting Information Fig. S2. The efficacy of compound **29c** to antagonize ER α was quite similar to Ful. When the *para*-hydroxyl group was replaced into *para*-methoxy, the antagonistic activity of **29f** decreased significantly to ER α , and **29f** also showed partial ER α agonistic ability. When changed trifluoroethyl group into ethyl group, **29i** decreased the ER α antagonistic activities, while the antagonist ability of ER β was enhanced.

2.5. Covalent SERDs degraded ER α ^{WT} and ER α ^{MUT}

All compounds were evaluated the degradation ability of ER α on MCF-7 cells. As shown in Fig. 5A, Series I and Series II compounds with OBHS backbone had no significant ER α degradation activity. Therefore, we mainly focused on ER α degradation ability of OBHSA skeleton-based compounds **29c–m** at concentrations of 1 or 5 μ mol/L, with Ful and **6a** as controls. The immunoblot results showed that compounds **29c**, **29i**, **29f**, **29h**, **29j** and **29m** could be effective in inducing ER α degradation at 1–5 μ mol/L. In particular, compounds **29c**, **29i** and **29f** exhibited an efficient ability to degrade ER α at 1 μ mol/L. The degradation ability of **29c** was more potent than other compounds at the same concentrations. The degradation activity was significantly affected by the compounds **29e**, **29g** and **29h**, in which the *para* hydroxy group of the sulfonamide was substituted. Compounds **29a–b**, regioisomer **29c'** and saturated analogue of **29k** showed impaired degradation ability.

In order to further characterize the effect of compound **29c** for ER α degradation, we examined the ER α degradation of compound **29c** at 0.5, 1 and 5 μ mol/L concentrations with 3, 6, 12 or 24 h treatment to determine the time course of its degradation in ER α ^{WT} and ER α ^{MUT} cell lines. Immunoblot analysis showed that ER α protein of MCF-7 cells was completely degraded by compound **29c** at 5 μ mol/L concentration over 24 h and LCC-2, T-47D, T-47D^{Y537S} and T-47D^{D538G} cell lines completely degraded by compound **29c** at 5 μ mol/L concentration over 12 h (Supporting Information Fig. S4). Meanwhile, the degradation by **29c** in a wide range of concentrations to determine the DC₅₀ (concentration causing 50% ER α degradation) values in BC cell lines. As shown in Fig. 5C, **29c** effectively induced ER α degradation in ER α ^{WT} and ER α ^{MUT} cell lines and DC₅₀ values were ranged from 0.01 to 0.05 μ mol/L, where **29c** had lower DC₅₀ values than Ful in MCF-7 and T-47D cell lines.

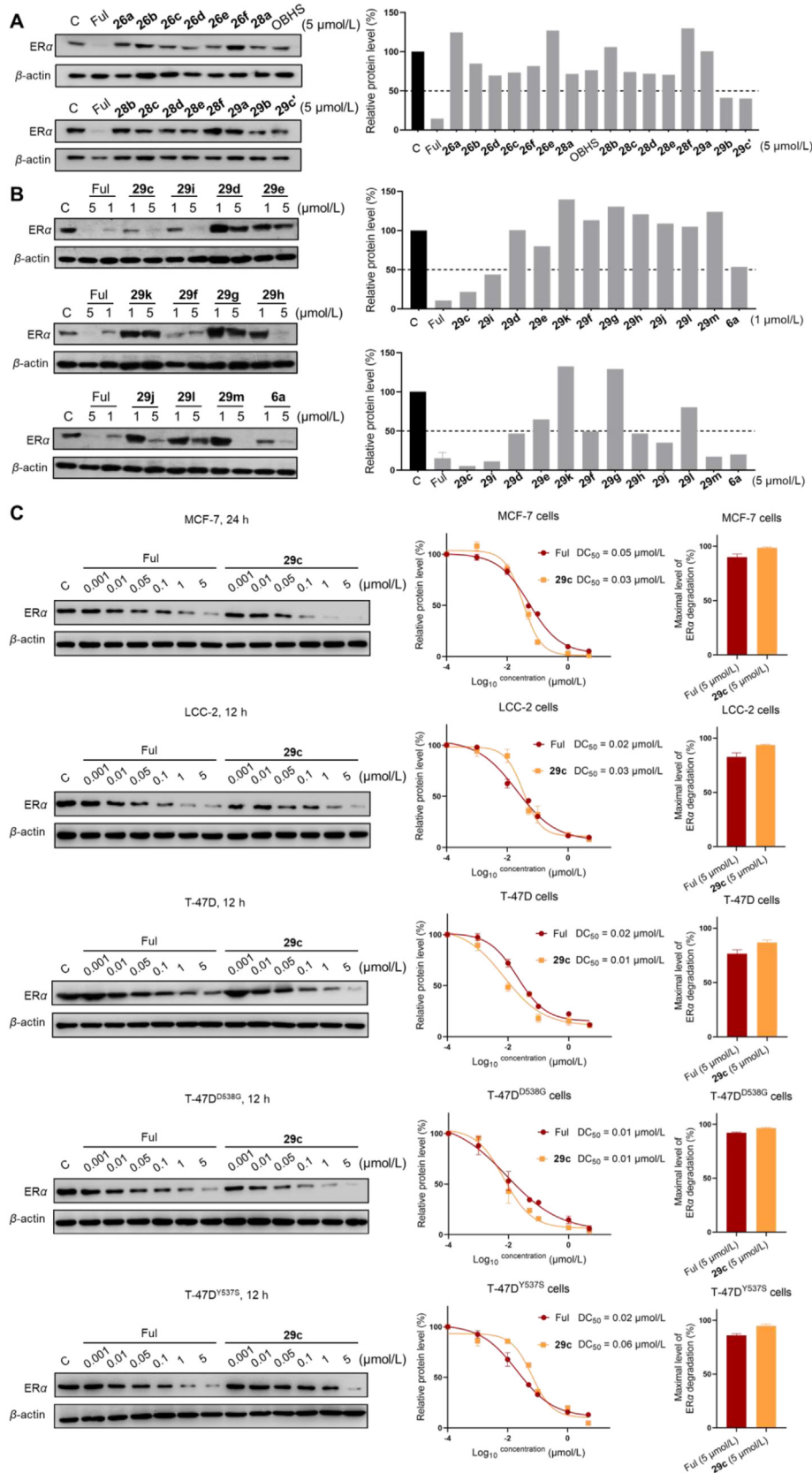


Figure 5 (A) Immunoblot analysis for ER α protein on the MCF-7 cells treated with indicated compounds at 5 $\mu\text{mol/L}$ for 24 h. (B) Immunoblot analysis of ER α protein on the MCF-7 cells treated with indicated compounds at 1 and 5 $\mu\text{mol/L}$. (C) Immunoblot analysis of ER α protein treated with gradient concentrations Ful or 29c in the indicated BC cell lines. DC₅₀ and D_{max} values were quantified from two independent experiments. All immunoblot was treated with β -actin as the loading control.

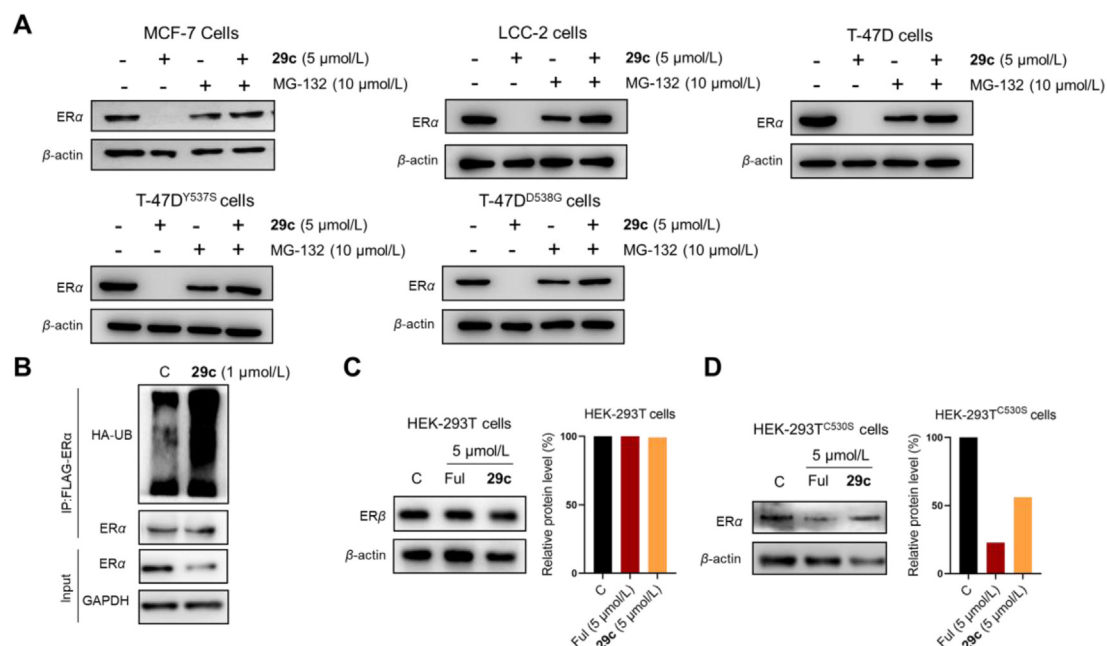


Figure 6 Further study of degradation of ER α protein by **29c**. (A) Intervention experiments of **29c** for ER α^{WT} and ER α^{MUT} in the indicated BC cell lines. (B) ER α ubiquitination assay. (C) Immunoblot analysis of ER β protein treated with **29c**. (D) Immunoblot analysis of ER α C530S mutant protein treated with **29c**.

Overall, the maximum degradation (D_{max}) capacity of **29c** was slightly higher than that of Ful at the endpoint of the assay.

The possible mechanism of action of compound **29c** mediated ER α degradation had been investigated (Fig. 6A) in ER α^{WT} and

ER α^{MUT} cell lines. Compound **29c** degraded ER α at 5 $\mu\text{mol/L}$, whereas 10 $\mu\text{mol/L}$ of the proteasome inhibitor MG-132 had no effect on ER α degradation. When treated with 10 $\mu\text{mol/L}$ MG-132 and 5 $\mu\text{mol/L}$ compound **29c**, the latter lost its ability to degrade

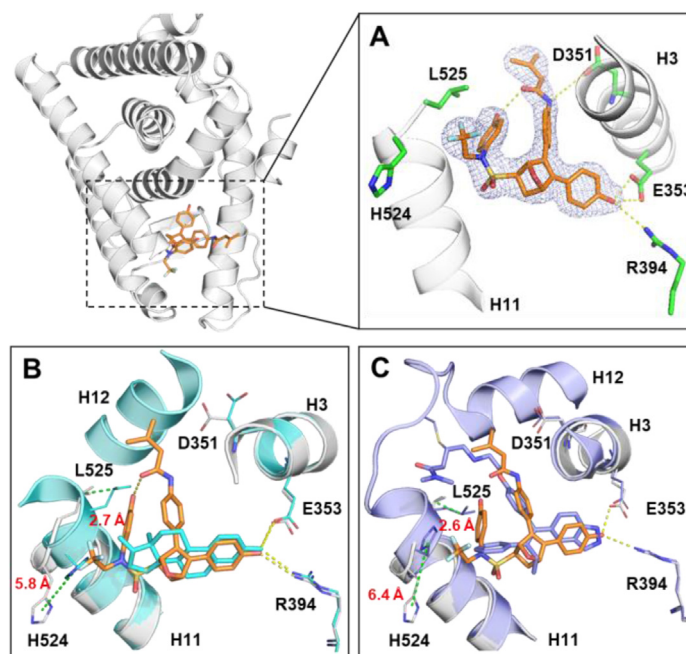


Figure 7 (A) The detailed complex (1S,2R,4S)-**29c** (orange) with ER α LBD (gray) interaction networks were shown in stereo view. The residues were presented as sticks (green). H-bonds were represented by yellow dotted lines. The $2F_o - F_c$ electron density map is contoured at 1σ . H11–12 loop region and H12 (528–547) could not be modeled due to very poor electron density. (B, C) Crystal structures of E₂-ER α (PDB: 3UUD, cyan) or H3B-5942-ER α (PDB: 6CHW, purple) were superposed with the **29c**-ER α structure (PDB: 7YMK), with the ligand shown as lines, distances (\AA) between H524 or L525 were indicated by dotted green lines.

Table 5 *In vivo* pharmacokinetic parameters of **29c** in female mice^a.

Route	Dose (mg/kg)	$t_{1/2}$ (h)	T_{max} (h)	C_{max} ($\mu\text{g/mL}$)	AUC ($\text{h}\cdot\mu\text{g/mL}$)	CL (mL/min/kg)	V_{ss} (L/kg)
iv	2	2.77	0.083	1.42	1.21	27.67	4.5
ip	4	6.38	0.167	0.352	0.96	—	—
po	20	5.81	0.5	0.153	0.36	—	—

^aThree plasma samples at each time point. $t_{1/2}$, half-life time; T_{max} , the maximum concentration of time point; C_{max} , compound maximum concentration in plasma samples; AUC, area under the concentration curve in plasma samples; CL, plasma clearance rate; V_{ss} , steady state volume of distribution; iv, intravenous administration; ip, intraperitoneal; po, oral administration.

ER α . Besides, we investigated the **29c** induced ubiquitination state of ER α through immunoprecipitant on experiments in the HEK-293T cells and identified K48-specific Ub-binding ER α proteins (Fig. 6B). These results suggested that degradation of ER α by **29c** is mediated by the proteasome.

Next, we also constructed the C530S plasmid bearing a single point mutation (C530 \rightarrow S530) that then transfected into HEK-293T cells. Meanwhile, we examined the antagonistic activity and ER α degradation ability of **29c** in HEK-293T^{C530S} cells, respectively. We found each of these abilities to be decreased in ER α C530S mutations. Combining the antiproliferative activity data and degradation profiles of the non-covalent derivative **29k**, those results demonstrated that C530 played a critical role in covalently targeting ER α with **29c**, while the non-covalent compound Ful was unaffected by this mutation (Table 4, entry 6 vs 1 and 7, Fig. 6D). The selective degradation of ER α by **29c** was also examined by transfection of ER β plasmid in HEK-293T cells, and immunoblot analysis showed that **29c** (5 $\mu\text{mol/L}$) had no degradation capacity for ER β (Fig. 6C). Finally, we performed a proteomic analysis to examine the level of global protein regulation by **29c**. The signaling pathways associated with endocrine resistance and breast cancer were significantly enriched through the Kyoto Encyclopedia of Genes and Genomes (KEGG) pathway enrichment analysis (Supporting Information Fig. S8).

2.6. Crystal structure and mass spectrometry analysis of **29c** in complex with ER α

To further clarify the detailed structural mechanism of **29c**, an in-house X-ray crystal structure was determined by soaking **29c** into ER α (Y537S/C381S/C417S) crystal (Fig. 7A) at resolution of 2.25 Å (PDB ID 7YMK, Supporting Information Table S2). Y537S mutation occurs frequently in endocrine-resistant BC. The structure analysis offers additional benefit of elucidating how **29c** behaves in a clinically relevant setting. While compounds were evaluated as racemates in the present study, high resolution X-ray structure shows only one chiral species with (1*S*,2*R*,4*S*)-configuration bound to ER α LBD. This demonstrates high stereospecificity of ER α in selecting a single enantiomer from a mixture for binding and activation. The crystal structure of the preferred (1*S*,2*R*,4*S*)-enantiomer showed even more dramatic effect on ER α , with H11-12 loop region and H12 (528–547) could not be modeled due to very poor electron density, demonstrating that H12 was highly disordered (Supporting Information Fig. S7). Biochemical and structural evidence indicates that the disorder or displacement of H12 is necessary for the binding of corepressors to generate a greater antagonism of proliferation^{18,41,43}.

Moreover, to confirm that C530 is the modification site, intact mass spectrometry analysis of substitutions was performed. Given

that there are three cystines (residues 417, 447, and 530) inside the ligand binding pocket of ER α , the control variable mutant ER α ^{Y537S} and ER α ^{Y537S C381S C417S} were analyzed. As expected, covalent adducts of ER α containing C530 were found to be detected (Supporting Information Fig. S6). These data confirm that **29c** was a small molecule targeting ER α that specifically and covalently bound to residue C530.

The more details on the crystal structure showed that **29c** adopts the desired antagonist conformation in the mutant context. The nitrogen of amino group of **29c** showed an H-bonding to D351 in H3, which would disrupt the H-bonding between D351 and S537 that contributes to the constitutive activity. The internal H-bond between the phenol of F ring and oxygen of amine group the caused **29c** to fold into a unique spatial conformation which helped orient the hydrophobic motif including trifluoroethyl group and F ring towards H11. Crystal complexes of **29c**–ER α superposed with the E₂–ER α structure were shown in Fig. 7B. The trifluoroethyl group strongly clashed with the H11 main chain agonist positioning of H524 and enforcing a 5.8 and 2.7 Å shift on H524 and L525 respectively. H524 and L525 on H11 were pushed to flip outwards, exposing hydrophobic patches that disturbs ER α protein homeostasis⁴⁰. When superposed with covalent antagonist H3B-5942 (Fig. 7B), it was shown that H524 and L525 were shifted 5.8 and 2.7 Å, respectively. These results suggested that H11 dislocation and H12 distortion of **29c** might be important to generate both ER antagonist and SERD profile.

2.7. Pharmacokinetic (PK) studies of **29c**

To evaluate the PK profiles of **29c** *in vivo*, **29c** was dosed to female Balb/c mice. Compound **29c** was administered *via* intravenous (iv, 2 mg/kg), intraperitoneal (ip, 4 mg/kg) or oral (*po*, 20 mg/kg). The PK data (Table 5) showed that the half-life ($t_{1/2}$) values of **29c** with ip and *po* administration were 6.38 and 5.81 h, respectively, and **29c** possessed a favorable drug exposure (C_{max} (iv): 1.42 $\mu\text{g/mL}$; C_{max} (ip): 0.352 $\mu\text{g/mL}$) in mice. Next, compound **29c** would be involved in pharmacodynamic studies in mice by ip administration due to insufficient oral bioavailability.

2.8. *In vivo* breast cancer model

Based on PK profiles of **29c**, MCF-7 tumor xenograft models in Balb/c nude mice were used to evaluate the antitumor efficacy of **29c** *in vivo* by intraperitoneal injection. As showed in Fig. 8, the **29c**-treated group at ip dose of 2 or 4 mg/kg had a significant tumor growth inhibition (TGI) activity. On Day 32, **29c** treatment at a dose of 4 mg/kg almost completely inhibited tumor growth (TGI = 92%), whereas TGI of tamoxifen at dose of 4 mg/kg and Ful at 2 mg/kg were 87% and 79%, respectively. There was no

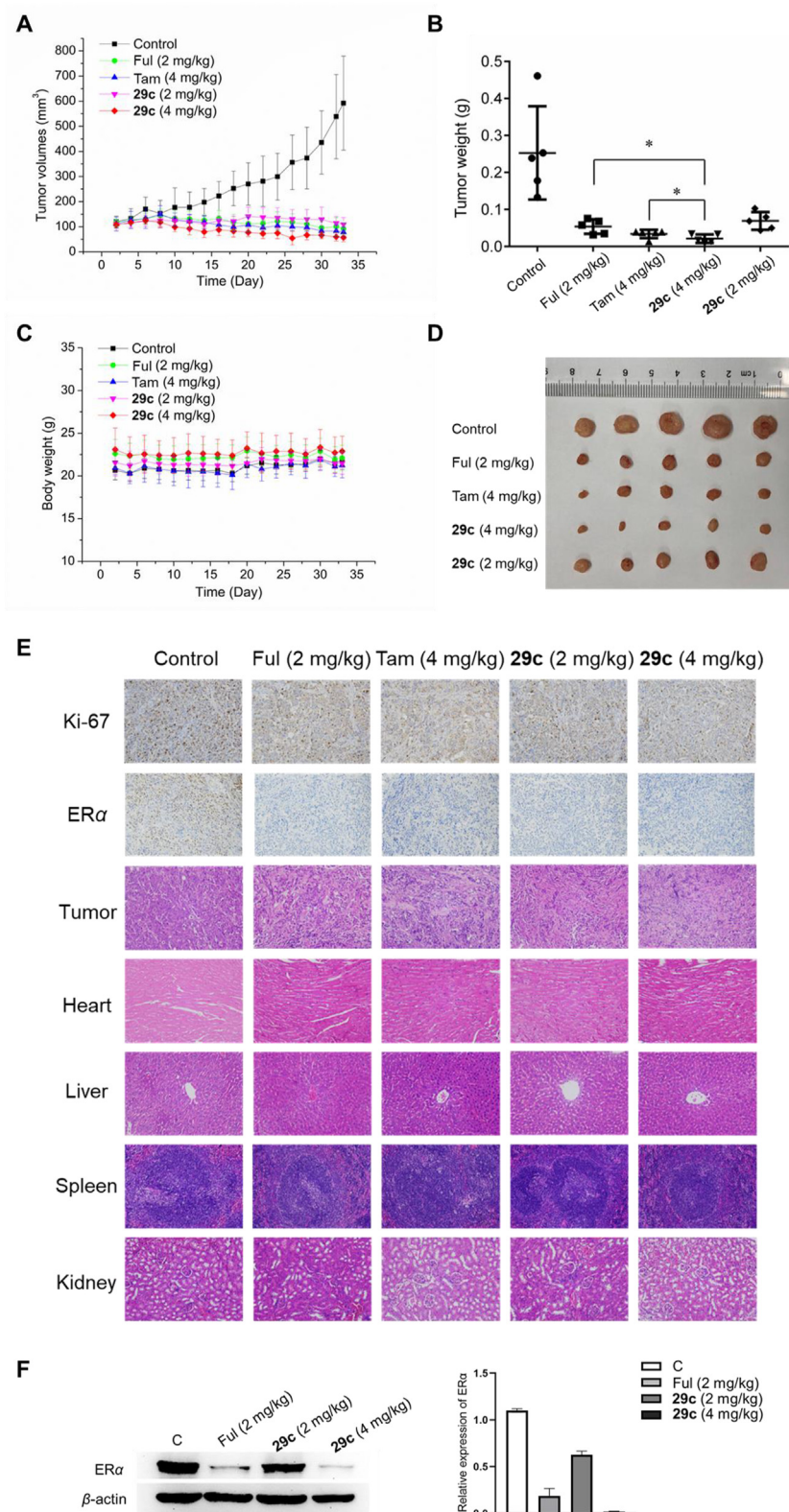


Figure 8 *In vivo* study in MCF-7 tumor BALB/c nude mice xenograft models by intraperitoneal injection once every 2 days. (A) Changes in tumor volume of mice were measured every 2 days. (B) Average weight of the dissected tumors in each group. (C) Body weight of mice were measured every 2 days ($*P < 0.05$). (D) Representative photos of the dissected tumors on Day 33. (E) Xenografted tumor tissues were stained (scale bar: 100 μ m) with Ki-67, ER α and H&E staining (scale bar: 50 μ m) of the heart, liver, spleen, and kidney from nude mice in the indicated groups after treatment. (F) Immunoblot analysis for detecting the expression of ER α in MCF-7 xenograft tumors.

statistically significant difference in tumor weight between **29c** and Ful treated control group at a dose of 2 mg/kg (Fig. 8B and D). The tumor proliferation marker protein Ki-67 staining and immunohistochemical (IHC) analysis indicated that **29c** significantly reduced tumor cell proliferation (Fig. 8E and Fig. S5A). Besides, **29c** did not apparently reduce mice body weight (Fig. 8C). Hematoxylin and eosin (H&E) analysis revealed that intraperitoneal administration of the compound **29c** did not show significant changes in the main visceral organs (Fig. 8E). These results indicated that **29c** possessed good safety and low toxicity to normal body tissues at efficacious doses. Additionally, ER α IHC analysis and Western-blot analysis also suggested that the high dose at 4 mg/kg of **29c** could significantly degrade ER α in MCF-7 xenograft tumors (Fig. 8F and Fig. S5B).

3. Conclusions

Endocrine-resistance remains a major challenge in ER α ⁺ breast cancer. There is an urgent need to develop novel drug with new mode to overcome acquired resistance. In this work, we developed a novel series of covalent selective estrogen receptor degraders (cSERDs) possessing the advantages of both covalent and degradation strategies. Herein, a highly potent cSERD **29c** is identified with superior anti-proliferative activity than Ful against ER α ⁺ BC cell lines of both wild and mutant types. Crystal structure and intact mass spectra of ER α -**29c** complex revealed that **29c** disrupted ER α protein homeostasis *via* covalently targeting C530 and strong hydrophobic interaction collided on H11, thus enforcing a unique antagonist conformation and driving the ER α degradation. These significant effects on ER α homeostasis do not occur directly *via* long side chains perturbing the morphology of H12 demonstrating a mechanism of action (MoA) distinct from typical ER α degraders. *In vivo*, **29c** has been shown to have potent anti-tumor activity in MCF-7 tumor xenograft models and low toxicity to normal body tissues. Overall, both *in vitro* and *in vivo*, compound **29c** holds promise for breast cancer treatment. This proof-of-principle study verifies that the development of novel ER α degraders combining indirect antagonism with covalent strategy, offering new opportunities for the development of innovative therapies for endocrine-resistant breast cancer treatment.

4. Experimental

4.1. General information

All reagents and solvents were available from commercial vendors. ¹H NMR and ¹³C NMR spectra with tetramethylsilane (TMS) internal standard were recorded on a Bruker Advance 400 MHz spectrometer. The chemical shifts were expressed in δ values (ppm). The monitoring of all reactions was thin-layer chromatography (TLC). Purifications were performed by column chromatography (200–300 mesh silica gel). All melting points were tested on RY-1G Tianjin Instruments. The mass raw data was acquired from Thermo Fisher Scientific and analyzed by Xcalibur™. HPLC (Shimadzu) conditions and results were shown in Supporting Information.

4.2. General procedure for target compounds **26a–g**, **28a–d** and **29a–j**

In a round-bottom flask, the furan derivatives (0.6 mmol) and dienophile derivatives (0.72 mmol) were added in THF

(1 mL). The mixture was stirred at 90 °C for 12 h under Ar balloon. The solvent was removed and the resulting residue was purified by column chromatography (DCM:MeOH, 50:1–20:1).

4-(Acrylamidophenyl-5,6-bis(4-hydroxyphenyl)-7-oxabicyclo[2.2.1]hept-5-ene-2-sulfonate (26a). 55% yield as yellow solid, mp 83–85 °C. ¹H NMR (400 MHz, acetone-*d*₆) δ 9.59 (s, 1H), 8.82 (d, *J* = 3.2 Hz, 1H), 8.75 (d, *J* = 3.0 Hz, 1H), 7.75 (d, *J* = 9.0 Hz, 2H), 7.25–7.19 (m, 6H), 6.81 (dd, *J* = 13.4, 8.6 Hz, 4H), 6.47–6.31 (m, 2H), 5.72 (dd, *J* = 9.7, 2.3 Hz, 1H), 5.64–5.62 (m, 1H), 5.43 (d, *J* = 4.3 Hz, 1H), 3.77 (dd, *J* = 8.3, 4.5 Hz, 1H), 2.40 (dt, *J* = 12.0, 4.4 Hz, 1H), 2.27 (dd, *J* = 12.1, 8.4 Hz, 1H). ¹³C NMR (100 MHz, acetone-*d*₆) δ 163.4, 162.32, 157.7, 157.5, 145.0, 141.3, 138.2, 136.9, 131.6, 129.2, 128.5, 126.7, 124.0, 123.2, 122.6, 120.6, 115.7, 115.5, 84.4, 82.7, 54.1, 19.8. HRMS (ESI) calcd. for C₂₇H₂₃NO₇S [M + Na]⁺ 528.1087, found 528.1088.

4-((E)-But-2-enamido)phenyl-5,6-bis(4-hydroxyphenyl)-7-oxabicyclo[2.2.1]hept-5-ene-2-sulfonate (26b). 81% yield as yellow solid, mp 86–89 °C. ¹H NMR (400 MHz, acetone-*d*₆) δ 9.41 (s, 1H), 8.78 (s, 2H), 7.75 (d, *J* = 9.0 Hz, 2H), 7.30–7.17 (m, 6H), 6.95–6.79 (m, 5H), 6.14 (dd, *J* = 15.0, 1.9 Hz, 1H), 5.65 (s, 1H), 5.44 (d, *J* = 4.3 Hz, 1H), 3.78 (dd, *J* = 8.3, 4.4 Hz, 1H), 2.42 (dt, *J* = 12.0, 4.4 Hz, 1H), 2.28 (dd, *J* = 12.1, 8.4 Hz, 1H), 1.89–1.85 (m, 3H). ¹³C NMR (100 MHz, acetone-*d*₆) δ 163.8, 157.6, 157.4, 144.9, 141.3, 140.6, 138.4, 137.0, 129.2, 128.6, 125.7, 124.1, 123.3, 122.6, 120.4, 115.7, 115.5, 84.4, 82.8, 60.5, 30.6, 16.9. HRMS (ESI) calcd. for C₂₈H₂₅NO₇S [M + Na]⁺ 542.1244, found 542.1246.

4-(3-Methylbut-2-enamido)phenyl-5,6-bis(4-hydroxyphenyl)-7-oxabicyclo[2.2.1]hept-5-ene-2-sulfonate (26c). 85% yield as yellow solid, mp 84–86 °C. ¹H NMR (400 MHz, CD₃OD) δ 7.54 (d, *J* = 9.0 Hz, 2H), 7.18–7.06 (m, 6H), 6.79–6.65 (m, 4H), 5.83 (s, 1H), 5.59 (d, *J* = 0.9 Hz, 1H), 5.34 (dd, *J* = 4.4, 1.3 Hz, 1H), 3.67 (dd, *J* = 8.4, 4.4 Hz, 1H), 2.41–2.34 (m, 1H), 2.19–2.11 (m, 4H), 1.89–1.85 (m, 3H). ¹³C NMR (100 MHz, CD₃OD) δ 166.2, 157.4, 157.3, 153.3, 144.9, 141.1, 137.9, 136.6, 129.0, 128.4, 123.7, 123.0, 122.3, 120.8, 118.2, 115.4, 115.2, 84.4, 82.8, 60.2, 53.5, 30.2, 26.2, 18.9. HRMS (ESI) calcd. for C₂₉H₂₇NO₇S [M + Na]⁺ 556.1400, found 556.1399.

4-Propiolamidophenyl-5,6-bis(4-hydroxyphenyl)-7-oxabicyclo[2.2.1]hept-5-ene-2-sulfonate(26d). 65% yield as yellow solid, mp 88–90 °C. ¹H NMR (400 MHz, acetone-*d*₆) δ 10.04 (s, 1H), 8.83–8.71 (m, 2H), 7.70 (d, *J* = 9.0 Hz, 2H), 7.26–7.21 (m, 6H), 6.84–6.78 (m, 4H), 5.64–5.62 (m, 1H), 5.43 (d, *J* = 4.3 Hz, 1H), 3.82–3.75 (m, 2H), 2.44–2.38 (m, 1H), 2.27 (dd, *J* = 12.1, 8.3 Hz, 1H). ¹³C NMR (100 MHz, acetone-*d*₆) δ 157.6, 157.5, 149.7, 145.6, 141.3, 137.3, 137.0, 129.2, 128.6, 124.1, 123.3, 122.8, 120.9, 115.7, 115.5, 84.3, 82.8, 77.7, 75.0, 60.6, 30.6. HRMS (ESI) calcd. for C₂₇H₂₁NO₇S [M + Na]⁺ 526.0931, found 526.0935.

4-(2-Chloroacetamido)phenyl-5,6-bis(4-hydroxyphenyl)-7-oxabicyclo[2.2.1]hept-5-ene-2-sulfonate (26e). 56% yield as yellow solid, mp 99–101 °C. ¹H NMR (400 MHz, acetone-*d*₆) δ 9.60 (s, 1H), 8.78–8.61 (m, 2H), 7.69 (d, *J* = 9.0 Hz, 2H), 7.27–7.18 (m, 6H), 6.85–6.74 (m, 4H), 5.63 (s, 1H), 5.43 (d, *J* = 4.3 Hz, 1H), 4.24 (s, 2H), 3.77 (dd, *J* = 8.3, 4.5 Hz, 1H), 2.44–2.37 (m, 1H), 2.30–2.23 (m, 1H). ¹³C NMR (100 MHz, acetone-*d*₆) δ 164.8, 157.6, 157.5, 145.4, 141.3, 137.5, 137.0, 129.2, 128.6, 124.0, 123.3, 122.7, 120.8, 115.7, 115.5, 84.4, 82.8, 60.6, 43.2, 30.6. HRMS (ESI) calcd. for C₂₆H₂₂ClNO₇S [M + Na]⁺ 550.0698, found 550.0699.

4-(2-Bromoacetamido)phenyl-5,6-bis(4-hydroxyphenyl)-7-oxabicyclo[2.2.1]hept-5-ene-2-sulfonate (**26f**). 60% yield as yellow solid, mp 102–104 °C. ¹H NMR (400 MHz, acetone-*d*₆) δ 9.75 (s, 1H), 8.79–8.62 (m, 2H), 7.68 (d, *J* = 9.0 Hz, 2H), 7.28–7.15 (m, 6H), 6.86–6.74 (m, 4H), 5.64–5.61 (m, 1H), 5.43 (d, *J* = 4.2 Hz, 1H), 4.03 (s, 2H), 3.77 (dd, *J* = 8.3, 4.5 Hz, 1H), 2.43–2.35 (m, 1H), 2.30–2.22 (m, 1H). ¹³C NMR (100 MHz, acetone-*d*₆) δ 164.8, 157.6, 157.4, 145.4, 141.3, 137.7, 137.0, 129.4, 129.2, 128.6, 124.1, 123.3, 122.7, 120.5, 115.7, 115.5, 84.4, 82.8, 60.6, 30.6. HRMS (ESI) calcd. for C₂₆H₂₂BrNO₇S [M + Na]⁺ 594.0193, found 594.0196.

Phenyl-5-(4-acrylamidophenyl)-6-(4-hydroxyphenyl)-7-oxabicyclo[2.2.1]hept-5-ene-2-sulfonate (**28a**, mixture of 3:1 isomers). 52% yield as yellow solid. ¹H NMR (400 MHz, CD₃OD) δ 7.64–7.55 (m, 2H), 7.41–7.07 (m, 10H), 6.80–6.71 (m, 2H), 6.48–6.33 (m, 2H), 5.80–5.72 (m, 1H), 5.66–5.56 (m, 1H), 5.40–5.27 (m, 1H), 3.81–3.63 (m, 1H), 2.58–2.35 (m, 1H), 2.28–2.05 (m, 1H). ¹³C NMR (100 MHz, CD₃OD) δ 164.7, 157.7, 149.3, 143.0, 138.2, 136.1, 131.0, 129.7, 128.6, 127.9, 127.0, 123.2, 121.9, 120.2, 115.3, 84.3, 82.8, 60.4, 29.3. HRMS (ESI) calcd. for C₂₇H₂₃NO₆S [M + Na]⁺ 512.1138, found 512.1133.

Phenyl-5-(4-((*E*)-but-2-enamido)phenyl)-6-(4-hydroxyphenyl)-7-oxabicyclo[2.2.1]hept-5-ene-2-sulfonate (**28b**, mixture of 5:1 isomers). 59% yield as yellow solid. ¹H NMR (400 MHz, CD₃OD) δ 7.59–7.45 (m, 2H), 7.36–6.95 (m, 10H), 6.93–6.81 (m, 1H), 6.74–6.61 (m, 2H), 6.15–5.93 (m, 1H), 5.63–5.47 (m, 1H), 5.34–5.21 (m, 1H), 3.78–3.55 (m, 4.4 Hz, 1H), 2.43–2.27 (m, 1H), 2.23–2.02 (m, 1H), 1.83 (d, *J* = 5.8 Hz, 3H). ¹³C NMR (100 MHz, CD₃OD) δ 165.3, 157.6, 149.3, 142.9, 141.3, 140.6, 138.5, 136.1, 129.7, 128.6, 125.1, 123.3, 122.6, 121.9, 120.1, 115.5, 115.3, 84.3, 82.8, 60.5, 30.0, 16.7. HRMS (ESI) calcd. for C₂₈H₂₅NO₆S [M + Na]⁺ 526.1294, found 526.1296.

Phenyl-6-(4-hydroxyphenyl)-5-(4-(3-methylbut-2-enamido)phenyl)-7-oxabicyclo[2.2.1]hept-5-ene-2-sulfonate (**28c**, mixture of 5:1 isomers). 67% yield as yellow solid. ¹H NMR (400 MHz, CD₃OD) δ 7.51–7.43 (m, 2H), 7.33–7.05 (m, 10H), 6.73–6.63 (m, 2H), 5.81 (d, *J* = 5.2 Hz, 1H), 5.60–5.50 (m, 1H), 5.36–5.22 (m, 1H), 3.71–3.56 (m, 1H), 2.43–2.29 (m, 1H), 2.20–2.06 (m, 4H), 1.85 (s, 3H). ¹³C NMR (100 MHz, CD₃OD) δ 166.3, 157.8, 153.1, 149.4, 142.7, 140.7, 138.8, 138.3, 136.2, 129.7, 128.6, 123.3, 122.6, 121.9, 119.9, 118.4, 115.5, 115.3, 84.3, 82.8, 60.1, 30.0, 29.4, 26.2, 18.8. HRMS (ESI) calcd. for C₂₉H₂₇NO₆S [M + Na]⁺ 540.1451, found 540.1452.

Phenyl-6-(4-(2-chloroacetamido)phenyl)-5-(4-hydroxyphenyl)-7-oxabicyclo[2.2.1]hept-5-ene-2-sulfonate (**28d**, mixture of 3:1 isomers). 43% yield as yellow solid. ¹H NMR (400 MHz, acetone-*d*₆) δ 9.57–9.50 (m, 1H), 8.74–8.66 (m, 1H), 7.67 (t, *J* = 8.9 Hz, 2H), 7.47–7.23 (m, 10H), 6.89–6.80 (m, 2H), 5.73–5.69 (m, 1H), 5.49 (td, *J* = 4.1, 1.2 Hz, 1H), 4.28–4.26 (m, 2H), 3.89–3.76 (m, 1H), 2.49–2.41 (m, 1H), 2.39–2.26 (m, 1H). ¹³C NMR (100 MHz, acetone-*d*₆) δ 164.6, 157.8, 149.6, 143.1, 140.9, 138.9, 138.2, 136.6, 129.9, 127.6, 123.7, 122.9, 122.3, 119.6, 115.8, 115.6, 84.4, 82.7, 60.5, 30.6. HRMS (ESI) calcd. for C₂₆H₂₂ClNO₆S [M + Na]⁺ 534.0749, found 524.0752.

Phenyl-5-(4-(2-bromoacetamido)phenyl)-6-(4-hydroxyphenyl)-7-oxabicyclo[2.2.1]hept-5-ene-2-sulfonate (**28e**, mixture of 3:1 isomers). 55% yield as yellow solid. ¹H NMR (400 MHz, CD₃OD) δ 7.57–7.47 (m, 2H), 7.38–7.10 (m, 10H), 6.79–6.69 (m, 2H), 5.56–5.66 (m, 1H), 5.42–5.29 (m, 1H), 3.96 (d, *J* = 5.3 Hz, 2H), 3.78–3.62 (m, 1H), 2.46–2.36 (m, 1H), 2.25–2.17 (m, 1H). ¹³C NMR (100 MHz, CD₃OD) δ 166.2, 157.7, 155.1, 149.4, 143.2, 140.5, 138.8, 137.9, 136.0, 129.7, 128.6, 123.2, 122.4, 121.9,

120.0, 115.5, 115.3, 84.3, 82.7, 60.4, 28.4. HRMS (ESI) calcd. for C₂₆H₂₂BrNO₆S [M + Na]⁺ 578.0243, found 578.0246.

4-Hydroxyphenyl-5-(4-hydroxyphenyl)-6-(4-(3-methylbut-2-enamido)phenyl)-7-oxabicyclo[2.2.1]hept-5-ene-2-sulfonate (**28f**, mixture of 3:1 isomer). 40% yield as yellow solid, mp 95–104 °C. ¹H NMR (400 MHz, CD₃OD) δ 7.54 (d, *J* = 8.5 Hz, 2H), 7.23 (dd, *J* = 26.4, 8.5 Hz, 4H), 6.99 (d, *J* = 8.9 Hz, 2H), 6.75 (dd, *J* = 36.6, 8.7 Hz, 4H), 5.88 (s, 1H), 5.64 (s, 1H), 5.42 (d, *J* = 3.4 Hz, 1H), 3.64 (dd, *J* = 8.3, 4.4 Hz, 1H), 2.48–2.43 (m, 1H), 2.20 (s, 4H), 1.93 (s, 3H). ¹³C NMR (100 MHz, CD₃OD) δ 166.3, 157.8, 156.3, 153.1, 141.8, 140.7, 138.6, 138.3, 129.2, 128.0, 127.2, 122.9, 122.6, 119.6, 118.3, 115.6, 115.5, 84.4, 82.6, 59.4, 30.2, 29.4, 26.2, 18.8. HRMS (ESI) calcd. for C₂₉H₂₇NO₇S [M + Na]⁺ 556.1400, found 556.1401.

N-(4-(3-(4-Hydroxyphenyl)-5-(*N*-(4-hydroxyphenyl)-*N*-(2,2,2-trifluoroethyl)sulfamoyl)-7-oxabicyclo[2.2.1]hept-2-en-2-yl)phenyl)acrylamide (**29a**). 55% yield as yellow solid, mp 110–111 °C. ¹H NMR (400 MHz, CD₃OD) δ 7.65 (d, *J* = 8.6 Hz, 2H), 7.35–7.24 (m, 2H), 7.21–7.06 (m, 4H), 6.76–6.62 (m, 4H), 6.51–6.37 (m, 2H), 5.84–5.77 (m, 1H), 5.51 (d, *J* = 1.2 Hz, 1H), 5.36 (dd, *J* = 4.4, 1.2 Hz, 1H), 4.40 (q, *J* = 8.6 Hz, 2H), 3.56–3.50 (m, 1H), 2.28–2.20 (m, 1H), 2.07–2.00 (m, 1H). ¹³C NMR (125 MHz, CD₃OD) δ 164.8, 157.6, 157.6, 142.9, 138.3, 136.3, 130.9, 130.2, 130.2, 128.3, 128.3, 128.1, 126.7, 124.2 (d, *J* = 279.7 Hz), 123.4, 120.2, 115.5, 115.2, 84.3, 82.7, 61.2, 52.1 (d, *J* = 34.0 Hz), 30.0. HRMS (ESI) calcd. for C₃₁H₂₉F₃N₂O₆S [M + Na]⁺ 609.1277, found 609.1279.

(*E*)-*N*-(4-(3-(4-Hydroxyphenyl)-5-(*N*-(4-hydroxyphenyl)-*N*-(2,2,2-trifluoroethyl)sulfamoyl)-7-oxabicyclo[2.2.1]hept-2-en-2-yl)phenyl)but-2-enamide (**29b**). 81% yield as yellow solid, mp 131–133 °C. ¹H NMR (400 MHz, CD₃OD) δ 7.59 (d, *J* = 8.6 Hz, 2H), 7.24 (d, *J* = 8.7 Hz, 2H), 7.12 (d, *J* = 8.7 Hz, 4H), 6.98–6.89 (m, 1H), 6.68 (t, *J* = 9.0 Hz, 4H), 6.13 (dd, *J* = 15.2, 1.7 Hz, 1H), 5.49–5.46 (m, 1H), 5.31 (d, *J* = 3.9 Hz, 1H), 4.37 (q, *J* = 8.5 Hz, 2H), 3.48–3.55 (m, 1H), 2.25–2.16 (m, 1H), 2.05–1.96 (m, 1H), 1.91 (dd, *J* = 6.9, 1.5 Hz, 3H). ¹³C NMR (100 MHz, CD₃OD) δ 165.4, 157.6, 157.5, 142.7, 141.4, 138.4, 136.2, 130.3, 130.2, 128.4, 128.1, 128.0, 125.6, 125.0, 124.2 (d, *J* = 281.8 Hz), 123.4, 122.8, 120.2, 115.6, 115.3, 84.3, 82.7, 61.3, 52.4 (d, *J* = 33.4 Hz), 30.1, 16.7. HRMS (ESI) calcd. for C₃₀H₂₇F₃N₂O₆S [M + Na]⁺ 623.1431, found 623.1434.

N-(4-(3-(4-Hydroxyphenyl)-5-(*N*-(4-hydroxyphenyl)-*N*-(2,2,2-trifluoroethyl)sulfamoyl)-7-oxabicyclo[2.2.1]hept-2-en-2-yl)phenyl)-3-methylbut-2-enamide (**29c**). 82% yield as yellow solid, mp 113–115 °C. ¹H NMR (400 MHz, CD₃OD) δ 7.56 (d, *J* = 8.6 Hz, 2H), 7.23 (d, *J* = 8.6 Hz, 2H), 7.12 (d, *J* = 8.8 Hz, 4H), 6.68 (t, *J* = 8.7 Hz, 4H), 5.88 (s, 1H), 5.31 (d, *J* = 4.1 Hz, 1H), 4.37 (q, *J* = 8.5 Hz, 2H), 3.49–3.54 (m, 1H), 2.39–2.15 (m, 4H), 2.04–1.95 (m, 1H), 1.92 (s, 3H). ¹³C NMR (100 MHz, CD₃OD) δ 166.3, 157.6, 157.5, 153.2, 142.6, 138.7, 136.3, 130.3, 130.2, 128.3, 128.1, 127.6, 124.2 (d, *J* = 280.8 Hz), 123.5, 119.9, 118.3, 115.6, 115.2, 84.3, 82.7, 61.3, 52.2 (d, *J* = 31.5 Hz), 30.1, 26.2, 18.8. HRMS (ESI) calcd. for C₃₁H₂₉F₃N₂O₆S [M + Na]⁺ 637.1590, found 637.1592.

N-(4-(3-(4-Hydroxyphenyl)-6-(*N*-(4-hydroxyphenyl)-*N*-(2,2,2-trifluoroethyl)sulfamoyl)-7-oxabicyclo[2.2.1]hept-2-en-2-yl)phenyl)-3-methylbut-2-enamide (**29c'**). 12% yield as yellow solid, mp 109–111 °C. ¹H NMR (400 MHz, CD₃OD) δ 7.50 (d, *J* = 8.5 Hz, 2H), 7.26–7.14 (m, 4H), 7.10 (d, *J* = 8.9 Hz, 2H), 6.80 (d, *J* = 8.7 Hz, 2H), 6.74–6.62 (m, 4H), 5.88–5.84 (m, 1H), 5.53–5.47 (m, 1H), 5.30 (dd, *J* = 4.4, 1.2 Hz, 1H), 4.37 (q, *J* = 8.5 Hz, 2H), 3.53–3.44 (m, 1H), 2.28–2.17 (m, 4H),

2.00–2.09 (m, 1H), 1.90 (s, 3H). ^{13}C NMR (100 MHz, CD_3OD) δ 166.3, 157.7, 157.6, 153.2, 149.8, 140.6, 138.5, 130.4, 130.1, 129.4, 128.2, 127.1, 124.2 (d, $J = 278.8$) 122.7, 119.7, 118.3, 115.7, 115.5, 115.5, 84.4, 82.6, 61.0, 52.2 (d, $J = 34.3$ Hz), 30.3, 26.2, 18.9. HRMS (ESI) calcd. for $\text{C}_{31}\text{H}_{29}\text{F}_3\text{N}_2\text{O}_6\text{S}$ [$\text{M} + \text{Na}$] $^+$ 637.1590, found 637.1592.

N-(4-(3-(4-Hydroxyphenyl)-6-(*N*-(*p*-tolyl)-*N*-(2,2,2-trifluoroethyl)sulfamoyl)-7-oxabicyclo[2.2.1]hept-2-en-2-yl)phenyl)-3-methylbut-2-enamide (**29d**). 35% yield as yellow solid, mp 85–87 °C. ^1H NMR (400 MHz, acetone- d_6) δ 9.20 (s, 1H), 8.83 (d, $J = 2.3$ Hz, 1H), 7.69–7.64 (m, 2H), 7.37–7.11 (m, 8H), 6.91–6.81 (m, 2H), 5.92–5.84 (m, 1H), 5.56 (d, $J = 1.2$ Hz, 1H), 5.38 (dd, $J = 4.3, 1.3$ Hz, 1H), 4.56 (q, $J = 8.7$ Hz, 2H), 3.57 (dd, $J = 8.3, 4.5$ Hz, 1H), 2.32 (s, 3H), 2.24–2.18 (m, 4H), 2.15–2.09 (m, 1H), 1.88 (d, $J = 1.3$ Hz, 3H). ^{13}C NMR (100 MHz, CD_3OD) δ 166.2, 157.8, 153.0, 140.6, 138.6, 138.5, 136.4, 129.7, 129.3, 128.5, 128.1, 127.1, 124.1 (d, $J = 279.2$ Hz), 122.7, 119.5, 118.3, 115.4, 84.4, 82.6, 61.1, 60.2 (d, $J = 31.3$ Hz), 30.2, 26.1, 19.7, 18.7. HRMS (ESI) calcd. for $\text{C}_{32}\text{H}_{31}\text{F}_3\text{N}_2\text{O}_5\text{S}$ [$\text{M} + \text{Na}$] $^+$ 635.1797, found 635.1798.

N-(4-(3-(4-Hydroxyphenyl)-6-(*N*-phenyl-*N*-(2,2,2-trifluoroethyl)sulfamoyl)-7-oxabicyclo[2.2.1]hept-2-en-2-yl)phenyl)-3-methylbut-2-enamide (**29e**). 35% yield as yellow solid, mp 88–90 °C. ^1H NMR (400 MHz, CD_3OD) δ 7.54–7.48 (m, 2H), 7.36–7.27 (m, 5H), 7.24–7.09 (m, 4H), 6.81–6.75 (m, 2H), 5.87 (d, $J = 1.3$ Hz, 1H), 5.51–5.48 (m, 1H), 5.35–5.29 (m, 1H), 4.53–4.40 (m, 2H), 3.50–3.45 (m, 1H), 2.25–2.18 (m, 4H), 2.07–2.00 (m, 1H), 1.94–1.90 (m, 3H). ^{13}C NMR (101 MHz, CD_3OD) δ 166.3, 157.7, 153.1, 140.6, 139.1, 138.6, 138.4, 129.3, 129.2, 128.7, 128.3, 128.1, 127.1, 124.1 (d, $J = 280.8$ Hz), 122.7, 119.6, 118.3, 115.5, 84.4, 82.6, 61.3, 51.9 (d, $J = 34.3$ Hz), 30.2, 26.2, 18.8. HRMS (ESI) calcd. for $\text{C}_{31}\text{H}_{29}\text{F}_3\text{N}_2\text{O}_5\text{S}$ [$\text{M} + \text{Na}$] $^+$ 621.1641, found 621.1643.

N-(4-(3-(4-Hydroxyphenyl)-5-(*N*-(4-methoxyphenyl)-*N*-(2,2,2-trifluoroethyl)sulfamoyl)-7-oxabicyclo[2.2.1]hept-2-en-2-yl)phenyl)-3-methylbut-2-enamide (**29f**). 77% yield as yellow solid, mp 114–117 °C. ^1H NMR (400 MHz, CD_3OD) δ 7.52 (d, $J = 8.7$ Hz, 2H), 7.25–7.16 (m, 6H), 6.80 (d, $J = 8.8$ Hz, 4H), 5.89–5.86 (m, 1H), 5.50–5.48 (m, 1H), 5.36–5.33 (m, 1H), 4.47–4.38 (m, 2H), 3.78 (s, 3H), 3.47–3.42 (m, 1H), 2.29–2.23 (m, 1H), 2.20 (d, $J = 1.3$ Hz, 3H), 2.10–2.03 (m, 1H), 1.93 (d, $J = 1.4$ Hz, 3H). ^{13}C NMR (100 MHz, CD_3OD) δ 166.2, 159.6, 157.8, 153.0, 140.6, 138.5, 138.5, 131.3, 130.2, 129.4, 127.0, 126.8 (d, $J = 283.0$ Hz), 122.75, 119.58, 118.3, 115.5, 114.2, 84.4, 82.6, 66.9, 60.9, 54.6, 51.4 (d, $J = 35.2$ Hz), 30.2, 26.2, 18.7. HRMS (ESI) calcd. for $\text{C}_{31}\text{H}_{29}\text{F}_3\text{N}_2\text{O}_5\text{S}$ [$\text{M} + \text{Na}$] $^+$ 621.1641, found 621.1645.

N-(4-(5-(*N*-(4-Fluorophenyl)-*N*-(2,2,2-trifluoroethyl)sulfamoyl)-3-(4-hydroxyphenyl)-7-oxabicyclo[2.2.1]hept-2-en-2-yl)phenyl)-3-methylbut-2-enamide (**29g**). 44% yield as yellow solid, mp 90–92 °C. ^1H NMR (400 MHz, CD_3OD) δ 7.52 (d, $J = 8.7$ Hz, 2H), 7.39–7.34 (m, 2H), 7.24 (d, $J = 8.6$ Hz, 2H), 7.20–7.16 (m, 2H), 7.08–7.02 (m, 2H), 6.80 (d, $J = 8.7$ Hz, 2H), 5.89–5.86 (m, 1H), 5.52–5.50 (m, 1H), 5.37 (d, $J = 4.3$ Hz, 1H), 4.48 (q, $J = 8.5$ Hz, 2H), 3.50–3.46 (m, 1H), 2.26–2.19 (m, 4H), 2.11–2.04 (m, 1H), 1.94 (d, $J = 1.4$ Hz, 3H). ^{13}C NMR (101 MHz, CD_3OD) δ 166.2, 162.2 (d, $J = 247.0$ Hz), 157.8, 153.1, 140.6, 138.6, 138.4, 135.2, 135.1, 131.0, 130.9, 129.3, 128.1, 127.1, 126.9 (d, $J = 289$ Hz), 122.7, 119.6, 118.3, 116.0, 115.7, 115.5, 84.4, 82.6, 61.5, 52.0 (d, $J = 35.0$ Hz), 30.2, 26.2,

18.7. HRMS (ESI) calcd. for $\text{C}_{31}\text{H}_{28}\text{F}_4\text{N}_2\text{O}_5\text{S}$ [$\text{M} + \text{Na}$] $^+$ 639.1547, found 639.1549.

N-(4-(3-(4-Hydroxyphenyl)-5-(*N*-(3-hydroxyphenyl)-*N*-(2,2,2-trifluoroethyl)sulfamoyl)-7-oxabicyclo[2.2.1]hept-2-en-2-yl)phenyl)-3-methylbut-2-enamide (**29h**). 77% yield as yellow solid, mp 114–117 °C. ^1H NMR (400 MHz, CD_3OD) δ 7.56 (d, $J = 8.5$ Hz, 2H), 7.22 (d, $J = 8.6$ Hz, 2H), 7.18–7.07 (m, 3H), 6.96–6.91 (m, 1H), 6.83–6.75 (m, 2H), 6.72 (d, $J = 8.6$ Hz, 2H), 5.90 (s, 1H), 5.51 (s, 1H), 5.35 (d, $J = 4.2$ Hz, 1H), 4.47 (q, $J = 9.0, 8.5$ Hz, 2H), 3.60–3.53 (m, 1H), 2.27–2.17 (m, 4H), 2.04–1.92 (m, 4H). ^{13}C NMR (100 MHz, CD_3OD) δ 166.3, 158.0, 157.5, 153.1, 142.6, 140.1, 138.7, 136.3, 129.8, 128.4, 127.8, 127.5, 124.1 (d, $J = 280.8$), 123.4, 119.9, 118.7, 118.3, 115.9, 115.3, 115.2, 84.3, 82.8, 61.7, 51.8 (d, $J = 34.3$ Hz), 30.1, 26.2, 18.8. HRMS (ESI) calcd. for $\text{C}_{31}\text{H}_{29}\text{F}_3\text{N}_2\text{O}_6\text{S}$ [$\text{M} + \text{Na}$] $^+$ 637.1590, found 623.1594.

N-(4-(5-(*N*-Ethyl-*N*-(4-hydroxyphenyl)sulfamoyl)-3-(4-hydroxyphenyl)-7-oxabicyclo[2.2.1]hept-2-en-2-yl)phenyl)-3-methylbut-2-enamide (**29i**). 82% yield as yellow solid, mp 121–123 °C. ^1H NMR (400 MHz, CD_3OD) δ 7.57 (d, $J = 8.6$ Hz, 2H), 7.26 (d, $J = 8.7$ Hz, 2H), 7.19–7.13 (m, 2H), 7.11–7.06 (m, 2H), 6.76–6.69 (m, 4H), 5.92–5.87 (m, 1H), 5.51–5.46 (m, 1H), 5.34 (d, $J = 3.7$ Hz, 1H), 3.80–3.69 (m, 2H), 3.52–3.47 (m, 1H), 2.28–2.19 (m, 4H), 2.06–2.00 (m, 1H), 1.93 (s, 3H), 1.06 (t, $J = 7.0$ Hz, 3H). ^{13}C NMR (100 MHz, CD_3OD) δ 166.3, 157.4, 157.1, 153.2, 142.3, 138.7, 136.5, 130.5, 129.8, 128.4, 127.9, 127.7, 123.6, 119.9, 118.3, 115.4, 115.2, 84.4, 82.8, 61.0, 46.6, 30.0, 26.2, 18.8, 13.6. HRMS (ESI) calcd. for $\text{C}_{31}\text{H}_{32}\text{N}_2\text{O}_6\text{S}$ [$\text{M} + \text{Na}$] $^+$ 583.1873, found 583.1876.

N-(4-(5-(*N*-Ethyl-*N*-(4-methoxyphenyl)sulfamoyl)-3-(4-hydroxyphenyl)-7-oxabicyclo[2.2.1]hept-2-en-2-yl)phenyl)-3-methylbut-2-enamide (**29j**). 69% yield as yellow solid, mp 92–94 °C. ^1H NMR (400 MHz, CD_3OD) δ 7.57 (d, $J = 8.7$ Hz, 2H), 7.31–7.21 (m, 2H), 7.22–7.12 (m, 4H), 6.88–6.81 (m, 2H), 6.75–6.69 (m, 2H), 5.90 (p, $J = 1.4$ Hz, 1H), 5.47 (d, $J = 1.2$ Hz, 1H), 5.34 (dd, $J = 4.4, 1.2$ Hz, 1H), 3.79–3.72 (m, 7H), 3.48 (dd, $J = 8.4, 4.4$ Hz, 1H), 2.29–2.19 (m, 4H), 2.04 (dd, $J = 12.1, 8.4$ Hz, 1H), 1.94 (d, $J = 1.4$ Hz, 3H), 1.07 (t, $J = 7.0$ Hz, 3H). ^{13}C NMR (100 MHz, CD_3OD) δ 166.3, 159.3, 157.5, 153.1, 142.3, 138.7, 136.5, 131.0, 130.4, 128.4, 127.9, 127.7, 123.6, 119.8, 118.3, 115.2, 114.0, 84.4, 82.8, 67.5, 61.0, 54.6, 29.9, 26.2, 25.1, 18.8, 13.6. HRMS (ESI) calcd. for $\text{C}_{32}\text{H}_{34}\text{N}_2\text{O}_6\text{S}$ [$\text{M} + \text{Na}$] $^+$ 597.2029, found 597.2033.

N-(4-((1*R*,4*R*)-3-(4-Hydroxyphenyl)-5-(*N*-(4-hydroxyphenyl)-*N*-(2,2,2-trifluoroethyl)sulfamoyl)-7-oxabicyclo[2.2.1]hept-2-en-2-yl)phenyl)-3-methylbutanamide (**29k**). 60% yield as yellow solid, mp 105–107 °C. ^1H NMR (400 MHz, CD_3OD) δ 7.56 (d, $J = 8.7$ Hz, 2H), 7.25 (d, $J = 8.7$ Hz, 2H), 7.21–7.06 (m, 4H), 6.78–6.62 (m, 4H), 5.54–5.42 (m, 2H), 5.33 (d, $J = 3.7$ Hz, 1H), 4.39 (q, $J = 8.5$ Hz, 2H), 3.59–3.50 (m, 1H), 2.29–2.13 (m, 4H), 2.06–1.96 (m, 1H), 1.03 (d, $J = 6.5$ Hz, 6H). ^{13}C NMR (100 MHz, CD_3OD) δ 172.8, 157.6, 157.5, 142.7, 138.3, 136.3, 130.3, 130.2, 128.3, 128.1, 127.9, 124.2 (d, $J = 280.8$ Hz), 123.4, 120.2, 115.6, 115.2, 84.3, 82.7, 61.3, 52.1 (d, $J = 34.3$ Hz), 45.8, 30.1, 26.2, 21.4. HRMS (ESI) calcd. for $\text{C}_{31}\text{H}_{31}\text{F}_3\text{N}_2\text{O}_6\text{S}$ [$\text{M} + \text{Na}$] $^+$ 639.1747, found 639.1749.

5-(4-Aminophenyl)-*N*,6-bis(4-hydroxyphenyl)-*N*-(2,2,2-trifluoroethyl)-7-oxabicyclo[2.2.1]hept-5-ene-2-sulfonamide (**29l**, mixture of 2:1 isomer). 82% yield as yellow solid. ^1H NMR (400 MHz, DMSO- d_6) δ 7.25–7.09 (m, 4H), 7.02 (t, $J = 9.3$ Hz,

2H), 6.82–6.66 (m, 4H), 6.54 (dd, $J = 22.7, 8.2$ Hz, 2H), 5.46 (d, $J = 17.1$ Hz, 1H), 5.32 (dd, $J = 14.8, 4.1$ Hz, 1H), 4.46 (d, $J = 9.2$ Hz, 2H), 3.54–3.38 (m, 1H), 2.12–1.84 (m, 2H). ^{13}C NMR (100 MHz, DMSO- d_6) δ 157.6, 141.6, 137.6, 134.9, 130.7, 130.4, 129.4, 129.1, 124.7 (d, $J = 281.8$ Hz), 124.3, 123.7, 120.0, 116.1, 115.8, 84.0, 82.3, 61.3, 52.4 (d, $J = 29.2$), 25.6. HRMS (ESI) calcd. for $\text{C}_{26}\text{H}_{23}\text{F}_3\text{N}_2\text{O}_5\text{S}$ [$\text{M} + \text{Na}$] $^+$ 555.1171, found 555.1174.

4-((5,6-bis(4-Hydroxyphenyl)-N-(2,2,2-trifluoroethyl)-7-oxabicyclo[2.2.1]hept-5-ene)-2-sulfonamido)phenyl 3-methylbut-2-enoate (**29m**). 55% yield as yellow solid, mp 108–111 °C. ^1H NMR (400 MHz, CD_3OD) δ 7.41–7.31 (m, 2H), 7.22–7.09 (m, 4H), 7.08–6.98 (m, 2H), 6.87–6.67 (m, 4H), 5.93 (dd, $J = 2.8, 1.4$ Hz, 1H), 5.47 (d, $J = 1.2$ Hz, 1H), 5.32–5.27 (m, 1H), 4.47 (q, $J = 8.5$ Hz, 2H), 3.58–3.45 (m, 1H), 2.28–2.15 (m, 4H), 2.08–1.95 (m, 4H). ^{13}C NMR (100 MHz, CD_3OD) δ 164.5, 161.3, 157.4, 157.2, 150.5, 141.0, 136.6, 136.3, 129.9, 129.4, 129.4, 129.2, 129.0, 128.2, 123.8, 123.1, 122.7, 122.6, 125.0 (d, $J = 280.1$ Hz), 115.4, 115.1, 114.8, 114.5, 114.2, 84.4, 82.7, 61.7, 52.0 (d, $J = 34.3$ Hz), 30.2, 26.3, 19.3. HRMS (ESI) calcd. for $\text{C}_{31}\text{H}_{28}\text{F}_3\text{NO}_7\text{S}$ [$\text{M} + \text{Na}$] $^+$ 638.1430, found 623.1436.

4.3. Estrogen receptor binding affinity

RBA values were detected *via* a competitive fluorometric binding experiment. Fluorescence tracer (40 nmol/L), human ER α or ER β LBD (0.8 $\mu\text{mol/L}$) and bovine gamma globulin (100 $\mu\text{g/mL}$) were dissolved in 100 mmol/L K_3PO_4 buffer (pH 7.4). All targeted compounds were diluted in different concentration with 100 mmol/L K_3PO_4 buffer and was mixed with the fluorescence tracer/ER complex solution. The mixture was excluded from light incubating for 2 h. Fluorescence polarization values were measured by BioTek reader. The values were mean \pm SD of at least three independent determinations.

4.4. Cell culture and cell viability assay

Human breast cancer cells MCF-7 and MCF-10A cells was purchased from the National Collection of Authenticated Cell Cultures (NCACC) and ATCC, respectively. Human tamoxifen-resistant breast cancer cell line (LCC-2), and T-47D/T-47D $^{\text{D538G/Y537S}}$ breast cancer cell lines were donated from the Wuhan University Medical Research Institute and Kaiwei Liang group at Wuhan University School of Basic Medical Sciences, respectively. MCF-7 or MCF-10A cell lines were cultured in DMEM medium (1% penicillin-streptomycin and 10% Fetal Bovine Serum). LCC-2, T-47D, T-47D $^{\text{D538G}}$ and T-47D $^{\text{Y537S}}$ cell lines were cultured in RPMI-1640 medium (1% penicillin-streptomycin and 10% Fetal Bovine Serum). Cells were planted in 96-well plates overnight and then incubated with different concentration of target compounds for 72 h. The cell lines viability was examined by Kit-8 (Biosharp, China). The IC_{50} was analyzed by GraphPad Prism 6.0 software. The procedure of apoptosis experiment was as follows: after a 48-h exposure to drug solutions, the cells were collected and subjected to staining with the FITC Annexin V Apoptosis Detection Kit I (BD Biosciences), as directed by the manufacturer. Subsequently, flow cytometry analysis was performed using a Beckman Coulter instrument.

4.5. Mass spectrometry to assess covalency of **29c**

ER α Y537S and C381S–C417S–Y537S proteins were incubated in 25 mmol/L Tris (pH = 8.0), 150 mmol/L NaCl, and 1 mmol/L TCEP with a 20-fold excess of compound (20 $\mu\text{mol/L}$ compound **29c** DMSO solution:1 $\mu\text{mol/L}$ ER α protein solution) at 4 °C overnight respectively. Intact protein was analyzed using an Agilent 1290 Infinity II LC coupled with a 6545-XT QTOF mass spectrometer. Mobile Phase A was water with 0.1% formic acid and Mobile Phase B was acetonitrile with 0.1% formic acid. Intact protein samples were separated with an PLRP-S biomolecules columns (1.0 mm \times 50 mm, 5 μm) employing 15 min gradient at a flow rate of 0.300 mL/min (5% B for 5 min, 5%–95% B for 5 min, 95% for 2 min, 95%–5% B for 0.1 min, 5% B for 2.9 min). The 6545-XT QTOF mass instrument parameters were set as the following: the dry gas flow rate was set 10.0 L/min at 325 °C, the nebulizer was set at 40 psig, the capillary voltage was set at 3.5 kV and the scan range was from 350 to 3000 m/z at 1 Hz. Data were collected with the MassHunter B.06.01 software.

4.6. Transcriptional activity assay

Human HEK-293T (ATCC) cells were seeded into 48-well plates with about 1×10^6 cells per well before transfection for 24 h. A solution of CaCl_2 (2.5 mol), pGL3-3ERE-tk (150 ng), pHAGE-puro-ER α (5 ng) or ER β (50 ng) or pET46EK-ER α^{C530S} , and pRL-cmv (1 ng) was adjusted to 12.5 μL and then mixed with an equal volume of $2 \times$ HBS buffer. Refreshed medium after 24 h of transfection which contained the desired concentrations of detected compounds. For detection of antagonistic activity, medium of dilute compound containing 10 nmol/L 17 β -estradiol was used to make the above concentrations for 24 h, and transcriptional activity was measured by a Stop & Glo Reagent.

4.7. Western blot assay

Western blot was conducted to analyze ER α protein levels on MCF-7, LCC-2, T-47D, T-47D $^{\text{Y537S}}$, T-47D $^{\text{D538G}}$ cells. Cells were planted in six-well plate and incubated with target compound (1 or 5 $\mu\text{mol/L}$) for indicated time. Cellular proteins were extracted using RIPA lysates and were separated by electrophoresis on SDS-PAGE gels. After the gel was transferred to the polyvinylidene fluoride (PVDF) membrane, it was blocked with 5% skim milk. Then PVDF membranes were incubated with mouse Anti- β -Actin antibody and rabbit anti-ER α antibody overnight. Membranes were washed and incubated with goat anti rabbit secondary antibody (Wuhan Feiyi Group, China) for 1 h. After washing, membranes were developed by ECL. For IP of tagged protein, Flag-ER α and HA-Ub plasmids (donated from the Wuhan University Medical Research Institute and Kaiwei Liang group at Wuhan University School of Basic Medical Sciences) were transfected into HEK-293T cells using Lipo2000 transfection reagent for 8–12 h. The basic medium (Opti-MEM) was replaced with complete medium (10% FBS) and incubated for another 12 h and the cells were collected and lysed with 1 mL of lysis buffer, followed by centrifugation at 21,000 rcf for 10 min at 4 °C. The supernatant was collected and the beads were mixed and washed twice with 1 mL of lysis buffer. The samples were then transferred

to each EP tube and followed by electrophoresis on SDS-PAGE gels as previously described.

4.8. Protein crystallization and data acquisition

Purifications of ER α and methods of crystallization were summarized in supporting information. All graphics for the protein structures were prepared by PyMOL. Atomic coordinates for the crystal structures of ER α with compounds **29c** (7YMK) can be accessed from the RCSB Protein Data Bank (www.rcsb.org).

4.9. PK studies in mice

PK Studies were conducted in BALB/c female mice ($n = 3$ mice/group). A solution of **29c** was prepared in Corn Oil and DMSO (95%:5%) for *po* administration (20 mg/kg), or in DMSO, PEG400, β -cyclodextrin, and saline (5%:40%:10%:45%) for *iv* administration (2 mg/kg), or in DMSO, PEG400 and saline (5%:40%:55%) for *ip*. administration (4 mg/kg). After administration, blood samples were collected at indicated time points of 0.25, 0.5, 1, 2, 4, 8, 12, 24 and 48 h respectively. The plasma samples were deproteinized with MeCN and concentration of each compound in supernatant was analyzed by LC/MS/MS.

4.10. Pharmacodynamic studies in nude mice

Female BALB/c nude mice (15–18 g, 5 weeks old) were purchased from Beijing HFK Bioscience Co. Ltd. All animal experiments are strictly followed the Guide for the Care and Use Committee at Wuhan University (permit no. S01320070A, Wuhan, China). 100 μ L PBS containing 1×10^7 MCF-7 cells were injected in the right axillary mammary fat pad area of mice. Once the tumor volume reached ~ 100 mm³, mice were randomly divided into four groups ($n = 5$ /group) and the conducted drug administration. The mice were intraperitoneally administered with vehicle control (PEG-400:DMSO:PBS = 40:5:55), Tam (4 mg/kg), Ful (2 mg/kg) or compound **29c** (2 or 4 mg/kg) every other day. The weight of the mice and the tumor volume were measured every 2 days. The formula for tumor size calculation: Volume = (Width)² \times (Length) \times 0.5. On Day 33, the mice were sacrificed. Tumor tissue sections Ki-67 were analyzed through immunohistochemistry and Western blot analysis. The heart, liver, spleen and kidney of mice were stained with H&E.

Acknowledgments

The work was supported by National Key R&D Program of China (2020YFA0908800, 2021YFC2100300), National Natural Science Foundation of China (82273774, 82073690, 81773557, 82173676, 82103994), the Fundamental Research Funds for the Central Universities of China (2042022kf0056), and the China Postdoctoral Science Foundation (2020M672435).

Author contributions

Chune Dong and Hai-Bing Zhou conceived and supervised the project. Yubo Wang, Xiangping Deng, Tian Feng, Hebing Hu, Xinyi Guo, Yan Chen, Baohua Xie and Yu Yang performed experiments. Yubo Wang, Jian Min, Xiangping Deng and Tian Feng are involved in acquisition of data, analysis and interpretation of data. Yubo Wang, Jian Min, Chun-Chi Chen, Rey-Ting Guo,

Chune Dong and Hai-Bing Zhou analyzed the data and wrote the manuscript. All authors read and approved the final manuscript.

Conflicts of interest

The authors declare no conflicts of interest.

Appendix A. Supporting information

Supporting data to this article can be found online at <https://doi.org/10.1016/j.apsb.2023.05.005>.

References

1. Siegel RL, Miller KD, Jemal A. Cancer statistics. *Ca - Cancer J Clin* 2020;**70**:7–30. 2020.
2. Tong CWS, Wu M, Cho WCS, To KKW. Recent advances in the treatment of breast cancer. *Front Oncol* 2018;**8**:227.
3. Anderson WF, Katki HA, Rosenberg PS. Incidence of breast cancer in the United States: current and future trends. *J Natl Cancer Inst* 2011;**103**:1397–402.
4. Eckhardt BL, Francis PA, Parker BS, Anderson RL. Strategies for the discovery and development of therapies for metastatic breast cancer. *Nat Rev Drug Discov* 2012;**11**:479–97.
5. Ariazi EA, Ariazi JL, Cordera F, Jordan VC. Estrogen receptors as therapeutic targets in breast cancer. *Curr Top Med Chem* 2006;**6**:181–202.
6. Gandhi N, Das GM. Metabolic reprogramming in breast cancer and its therapeutic implications. *Cells* 2019;**8**:89.
7. Ciruelos E, Pascual T, Arroyo Vozmediano ML, Blanco M, Manso L, Parrilla L, et al. The therapeutic role of fulvestrant in the management of patients with hormone receptor-positive breast cancer. *Breast* 2014;**23**:201–8.
8. Lin X, Xiang H, Luo G. Targeting estrogen receptor α for degradation with PROTACs: a promising approach to overcome endocrine resistance. *Eur J Med Chem* 2020;**206**:112689.
9. Lu Y, Liu W. Selective estrogen receptor degraders (SERDs): a promising strategy for estrogen receptor positive endocrine-resistant breast cancer. *J Med Chem* 2020;**63**:15094–114.
10. Lai A, Kahraman M, Govek S, Nagasawa J, Bonnefous C, Julien J, et al. Identification of GDC-0810 (ARN-810), an orally bioavailable selective estrogen receptor degrader (SERD) that demonstrates robust activity in tamoxifen-resistant breast cancer xenografts. *J Med Chem* 2015;**58**:4888–904.
11. Hu J, Hu B, Wang M, Xu F, Miao B, Yang CY, et al. Discovery of ERD-308 as a highly potent proteolysis targeting chimera (PROTAC) degrader of estrogen receptor (ER). *J Med Chem* 2019;**62**:1420–42.
12. Lu Z, Cao Y, Zhang D, Meng X, Guo B, Kong D, et al. Discovery of thieno[2,3-*e*]indazole derivatives as novel oral selective estrogen receptor degraders with highly improved antitumor effect and favorable druggability. *J Med Chem* 2022;**65**:5724–50.
13. Lai AC, Crews CM. Induced protein degradation: an emerging drug discovery paradigm. *Nat Rev Drug Discov* 2017;**16**:101–14.
14. Robertson JFR, Bondarenko IM, Trishkina E, Dvorkin M, Panasci L, Manikhas A, et al. Fulvestrant 500 mg versus anastrozole 1 mg for hormone receptor-positive advanced breast cancer (FALCON): an international, randomised, double-blind, phase 3 trial. *Lancet* 2016;**388**:2997–3005.
15. Howell A, Sapunar F. Fulvestrant revisited: efficacy and safety of the 500-mg dose. *Clin Breast Cancer* 2011;**11**:204–10.
16. McDonnell DP, Wardell SE, Norris JD. Oral selective estrogen receptor downregulators (SERDs), a breakthrough endocrine therapy for breast cancer. *J Med Chem* 2015;**58**:4883–7.
17. Hernando C, Ortega-Morillo B, Tapia M, Moragón S, Martínez MT, Eroles P, et al. Oral selective estrogen receptor degraders (SERDs) as a

- novel breast cancer therapy: present and future from a clinical perspective. *Int J Mol Sci* 2021;**22**:7812.
18. Fanning SW, Mayne CG, Dharmarajan V, Carlson KE, Martin TA, Novick SJ, et al. Estrogen receptor α somatic mutations Y537S and D538G confer breast cancer endocrine resistance by stabilizing the activating function-2 binding conformation. *Elife* 2016;**5**:e12792.
 19. Wang L, Sharma A. The quest for orally available selective estrogen receptor degraders (SERDs). *ChemMedChem* 2020;**15**:2072–97.
 20. Kiely-Collins H, Winter GE, Bernardes GJL. The role of reversible and irreversible covalent chemistry in targeted protein degradation. *Cell Chem Biol* 2021;**28**:952–68.
 21. Abdeldayem A, Raouf YS, Constantinescu SN, Moriggl R, Gunning PT. Advances in covalent kinase inhibitors. *Chem Soc Rev* 2020;**49**:2617–87.
 22. Singh J, Petter RC, Baillie TA, Whitty A. The resurgence of covalent drugs. *Nat Rev Drug Discov* 2011;**10**:307–17.
 23. De Vita E. 10 years into the resurgence of covalent drugs. *Future Med Chem* 2021;**13**:193–210.
 24. Boike L, Henning NJ, Nomura DK. Advances in covalent drug discovery. *Nat Rev Drug Discov* 2022:1–18.
 25. Furman C, Hao MH, Prajapati S, Reynolds D, Rimkunas V, Zheng GZ, et al. Estrogen receptor covalent antagonists: the best is yet to come. *Cancer Res* 2019;**79**:1740–5.
 26. Furman C, Puyang X, Zhang Z, Wu ZJ, Banka D, Aithal KB, et al. Covalent ER α antagonist H3B-6545 demonstrates encouraging pre-clinical activity in therapy-resistant breast cancer. *Mol Cancer Therapeut* 2022;**21**:890–902.
 27. Puyang X, Furman C, Zheng GZ, Wu ZJ, Banka D, Aithal K, et al. Discovery of selective estrogen receptor covalent antagonists for the treatment of ER α ^{WT} and ER α ^{MUT} breast cancer. *Cancer Discov* 2018;**8**:1176–93.
 28. Hamilton EP, Wang JS, Pluard TJ, Johnston SRD, Morikawa A, Dees EC, et al. Phase I/II study of H3B-6545, a novel selective estrogen receptor covalent antagonist (SERCA), in estrogen receptor positive (ER⁺), human epidermal growth factor receptor 2 negative (HER2⁻) advanced breast cancer. *J Clin Oncol* 2021;**39**:1018.
 29. Zhou HB, Comminos JS, Stossi F, Katzenellenbogen BS, Katzenellenbogen JA. Synthesis and evaluation of estrogen receptor ligands with bridged oxabicyclic cores containing a diarylethene motif: estrogen antagonists of unusual structure. *J Med Chem* 2005;**48**:7261–74.
 30. Ning W, Hu Z, Tang C, Yang L, Zhang S, Dong C, et al. Novel hybrid conjugates with dual suppression of estrogenic and inflammatory activities display significantly improved potency against breast cancer. *J Med Chem* 2018;**61**:8155–73.
 31. Tang C, Li C, Zhang S, Hu Z, Wu J, Dong C, et al. Novel bioactive hybrid compound dual targeting estrogen receptor and histone deacetylase for the treatment of breast cancer. *J Med Chem* 2015;**58**:4550–72.
 32. Deng X, Xie B, Li Q, Xiao Y, Hu Z, Deng X, et al. Discovery of novel bicyclic bhenylselenyl-containing hybrids: an orally bioavailable, potential, and multiacting class of estrogen receptor modulators against endocrine-resistant breast cancer. *J Med Chem* 2022;**65**:7993–8010.
 33. Aliau S, Matras H, Richard E, Borgna JL. Cysteine 530 of the human estrogen receptor alpha is the main covalent attachment site of 11 β -(aziridinylalkoxyphenyl)estradiols. *Biochemistry* 1999;**38**:14752–62.
 34. Katzenellenbogen JA. The 2010 Philip S. Portoghesi medicinal chemistry lectureship: addressing the "core issue" in the design of estrogen receptor ligands. *J Med Chem* 2011;**54**:5271–82.
 35. Weerapana E, Wang C, Simon GM, Richter F, Khare S, Dillon MB, et al. Quantitative reactivity profiling predicts functional cysteines in proteomes. *Nature* 2010;**468**:790–5.
 36. Nacht M, Qiao L, Sheets MP, St Martin T, Labenski M, Mazdiyasn H, et al. Discovery of a potent and isoform-selective targeted covalent inhibitor of the lipid kinase PI3K α . *J Med Chem* 2013;**56**:712–21.
 37. Hu Z, Li Y, Xie B, Ning W, Xiao Y, Huang Y, et al. Novel class of 7-oxabicyclo[2.2.1]heptene sulfonamides with long alkyl chains displaying improved estrogen receptor α degradation activity. *Eur J Med Chem* 2019;**182**:111605.
 38. Li Y, Zhang S, Zhang J, Hu Z, Xiao Y, Huang J, et al. Exploring the PROTAC degron candidates: OBHSA with different side chains as novel selective estrogen receptor degraders (SERDs). *Eur J Med Chem* 2019;**172**:48–61.
 39. Zheng Y, Zhu M, Srinivasan S, Nwachukwu JC, Cavett V, Min J, et al. Development of selective estrogen receptor modulator (SERM)-like activity through an indirect mechanism of estrogen receptor antagonism: defining the binding mode of 7-oxabicyclo[2.2.1]hept-5-ene scaffold core ligands. *ChemMedChem* 2012;**7**:1094–100.
 40. Srinivasan S, Nwachukwu JC, Bruno NE, Dharmarajan V, Goswami D, Kastrati I, et al. Full antagonism of the estrogen receptor without a prototypical ligand side chain. *Nat Chem Biol* 2017;**13**:111–8.
 41. Fanning SW, Jeselsohn R, Dharmarajan V, Mayne CG, Karimi M, Buchwalter G, et al. The SERM/SERD bazedoxifene disrupts ESR1 helix 12 to overcome acquired hormone resistance in breast cancer cells. *Elife* 2018;**7**:e37161.
 42. Wang C, Li C, Zhou H, Huang J. High-throughput screening assays for estrogen receptor by using coumestrol, a natural fluorescence compound. *J Biomol Screen* 2014;**19**:253–8.
 43. Min J, Nwachukwu JC, Min CK, Njeri JW, Srinivasan S, Rangarajan ES, et al. Dual-mechanism estrogen receptor inhibitors. *Proc Natl Acad Sci U S A* 2021;**118**:e2101657118.